SYNTHESIS AND CHARACTERIZATION OF GRAPHENE SHEETS

By

Qurat-Ul-Ain

(160-FBAS/MSPHY/S13)

DEPARTMENT OF PHYSICS

FACULTY OF BASIC AND APPLIED SCIENCES,

INTERNATIONAL ISLAMIC UNIVERSITY,

ISLAMABAD

(2015)

Physics

Energy Physics

SYNTHESIS AND CHARACTERIZATION OF GRAPHENE SHEETS

By

Qurat-Ul-Ain
(160-FBAS/MSPHY/S13)

Supervisor

Dr. Shamaila Sajjad

Co-Supervisor

Dr. Sajjad Leghari

DEPARTMENT OF PHYSICS

FACULTY OF BASIC AND APPLIED SCIENCES,

INTERNATIONAL ISLAMIC UNIVERSITY,

ISLAMABAD

(2015)

INTERNATIONAL ISLAMIC UNIVERSITY, ISLAMABAD

FACULTY OF BASIC AND APPLIED SCIENCES

DEPARTMENT OF PHYSICS

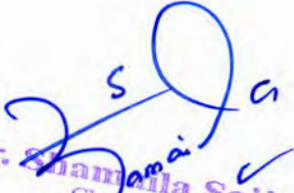# SYNTHESIS AND CHARACTERIZATION OF GRAPHENE SHEETS

By

Qurat-Ul-Ain

(Registration No. 160-FBAS/MSPHY/S13)

A thesis submitted to

Department of Physics

for the award of the degree of

MS Physics

Signature: _____

(Chairperson, Department of Physics)

Signature: _____

(Dean FBAS, IIU, Islamabad)

INTERNATIONAL ISLAMIC UNIVERSITY, ISLAMABAD
FACULTY OF BASIC AND APPLIED SCIENCES
DEPARTMENT OF PHYSICS

Dated:08-04-2015

FINAL APPROVAL

It is certified that the work presented in this thesis entitled "**SYNTHESIS AND CHARACTERIZATION OF GRAPHENE SHEETS**" by **MS. QURAT-UL-AIN** bearing **Registration No. 160-FBAS/MSPHY/S13**is of sufficient standard in scope and quality for the award of degree of MS Physics from International Islamic University, Islamabad.

COMMITTEE

External Examiner

Dr. GHAZANFAR ABBAS
Assistant Professor,
Department of Physics,
COMSATS Institute of Information Technology (CIIT),
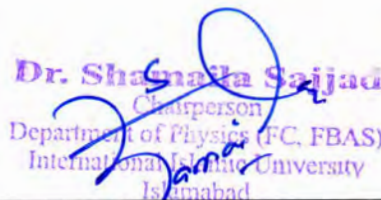Islamabad.

Internal Examiner

Dr. SADAF JAMIL
Assistant Professor,
Department of Physics, FBAS, IIUI.

Supervisor

Dr. SHAMAILA SAJJAD
Assistant Professor/Chairperson
Department of Physics, FBAS, IIUI.

Dr. Shamaila Sajjad
Chairperson
Department of Physics (FC, FBAS)
International Islamic University
Islamabad

Co-supervisor

Dr. SAJJAD AHMED KHAN LEGHARI
Principal Scientist, PAEC, Islamabad.

A thesis submitted to

Department of Physics

International Islamic University Islamabad

as a partial fulfillment for the award of the degree of

MS in Physics

Declaration

I hereby declare that this thesis work, neither as a whole nor a part of it has been copied out from any source. Further, work presented in this dissertation has not been submitted in support of any application for any other degree or qualification to any other university or institute and is considerable under the plagiarism rules of Higher Education Commission (HEC), Pakistan.

Qurat-Ul-Ain

Qurat-Ul-Ain

(160-FBAS/MSPHY/S13)

Dedication

I would like to dedicate this thesis to my beloved parents and whole family

for their endless love, support and encouragement throughout my life.

Acknowledgement

Qurat-Ul-Ain

(160-FBAS/MSPHY/S13)

List of Figures

List of Tables

List of Abbreviations

AFM	Atomic Force Microscopy
BET	Brunauer-Emmett-Teller
CNTs	Carbon Nanotubes
EDS	Energy Dispersive Spectroscopy
FESEM	Field Emission Spectroscopy
FOLED	Flexible Organic Light Emitting Diodes
FTIR	Fourier Transform Infrared Spectroscopy
GA	Graphene Sheets prepared by using Ammonia as a reducing agent
GM	Graphene Sheets synthesized by Microwave Synthesis Method
GNs	Graphene nanosheets
GO	Graphene Oxide
GP	Graphene Sheets prepared by using Plant Extract as a reducing agent
GtO	Graphite Oxide
LLs	Landau levels
MB	Methylene Blue
MWNTs	Multi Walled Nanotubes
nm	Nanometer
RGO	Reduced Graphene Oxide
RhB	Rhodamine B
SAED	Selective Area Electron Diffraction
SEM	Scanning Electron Microscopy
SWNTs	Single Walled Nanotubes
TEM	Transmission Electron Microscopy
XPS	X-ray photoelectron spectroscopy
XRD	X-Ray Diffraction

Abstract

Graphene nanosheets has been synthesized by Hummers method and microwave synthesis method. Ammonium hydroxide and plant extract are used in comparison to reduce the graphene oxide in Hummers method. Graphene oxide (GO) and graphene sheets are incorporated with copper oxide (CuO) nanoparticles for the application of photo-catalysis. Study on photo-catalytic activity of as-synthesized nanocomposites including the photo-degradation of methylene blue (MB) under UV light irradiation. To analyze the synthesized graphene nanosheets X-ray diffraction spectroscopy, scanning electron microscopy, energy dispersive x- ray spectroscopy and Fourier transform infra-red spectroscopy are used. XRD results of prepared graphene samples revealed that graphene prepare by ammonia has nearly the same reduction level as that prepared by plant extract. Peak intensity graphene prepared by ammonia is greater with (002) plane at $2\theta = 25.77°$ than graphene prepared by plant extract at same angle and with the same plane indicating that graphene prepared by plant extract is more amorphous than graphene prepared by ammonia. SEM results obtained from synthesized sample showed that graphene nanosheets has ultra-thin layered, crumpled and wrinkled morphology. Graphene sheets are more transparent than graphene oxide sheets. FTIR spectroscopy confirmed the oxidation and reduction processes during synthesis. The as-synthesized CuO/ graphene nanocomposite exhibits the better photo-catalytic performance for the degradation of methylene blue than pure CuO nanoparticles.

Chapter No. 1

Introduction

1.1 Nanoscience and Nanotechnology:

In 1959 Richard Feynman gives the concept of a new field, he said that "there is plenty of room at the bottom" in the conference of the American Physical Society. In 1965 he gets noble price in physics on his fantastic achievement. In nanoscience, things can handle at very small scale. With the development of this new field, people start their efforts to fabricate and characterize the old and new materials at nanoscale which make nanotechnology an interesting field of study [1]. Nanotechnology has applications in many fields within physics, chemistry and biology, to synthesize and control the structures in which their dimensions are ranging from a few nanometers to less than 100 nanometers.
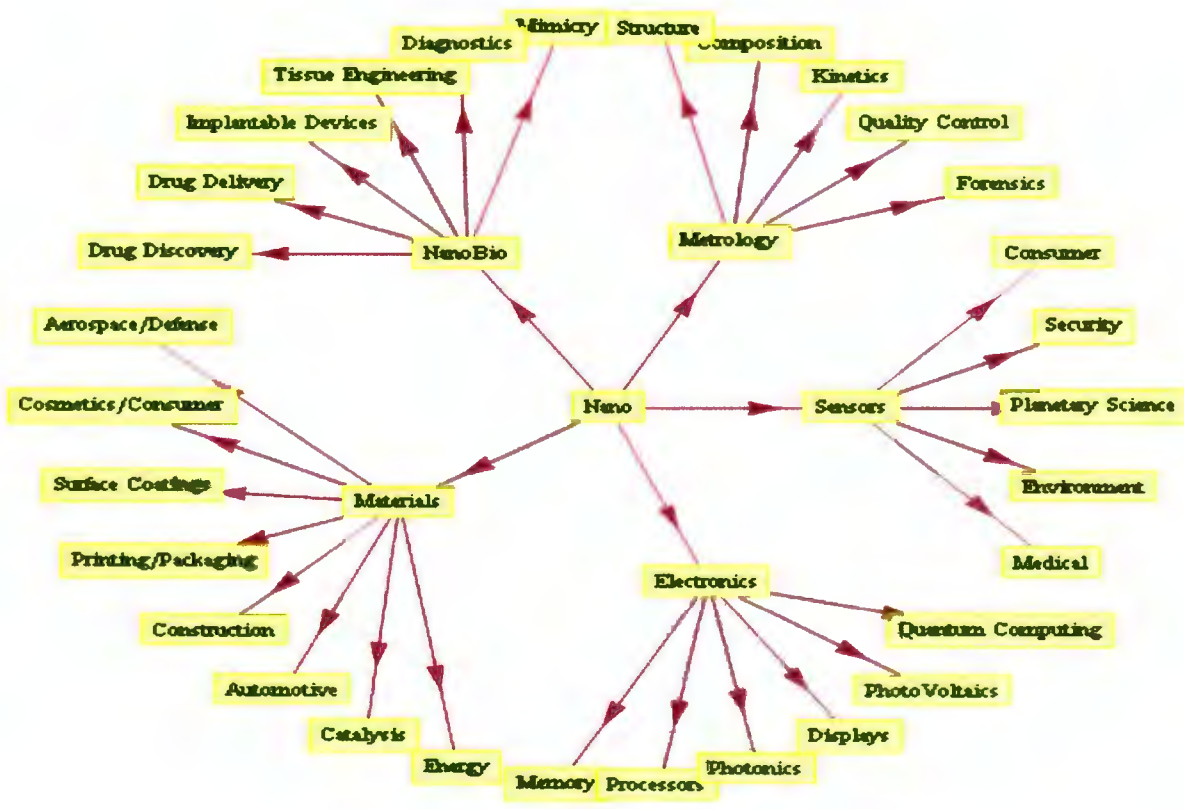
Figure 1.1: Applications of nanotechnology

In chemistry, nanoscience is related to the colloids, micelles, and polymer molecules, phase-separated regions in block copolymers, very large molecules, or aggregates of many molecules. Recently, structures such as buckytubes, silicon nanorods, and compound semiconductor quantum dots have emerged as fascinating categories of nanostructures. In physics and electrical engineering, this range of sizes has been associated with the quantum behavior, and the behavior of electrons and photons in nanoscale structures. Biology and biochemistry also have a great interest in nanostructures as components of the cell. In biology, from DNA and viruses to sub cellular organelles and gap junctions can be considered as nanostructures [2].

1.2 Carbon and its allotropes:

Carbon is the most important material of the periodic table. Depending upon its flexible bonding, there are many allotropes of carbon, diamond and graphite are very old material. Ten to twenty years ago, fullerenes and nanotubes were discovered. More recently the two-dimensional form graphene was obtained, which is very attractive material due to its excellent properties [3].
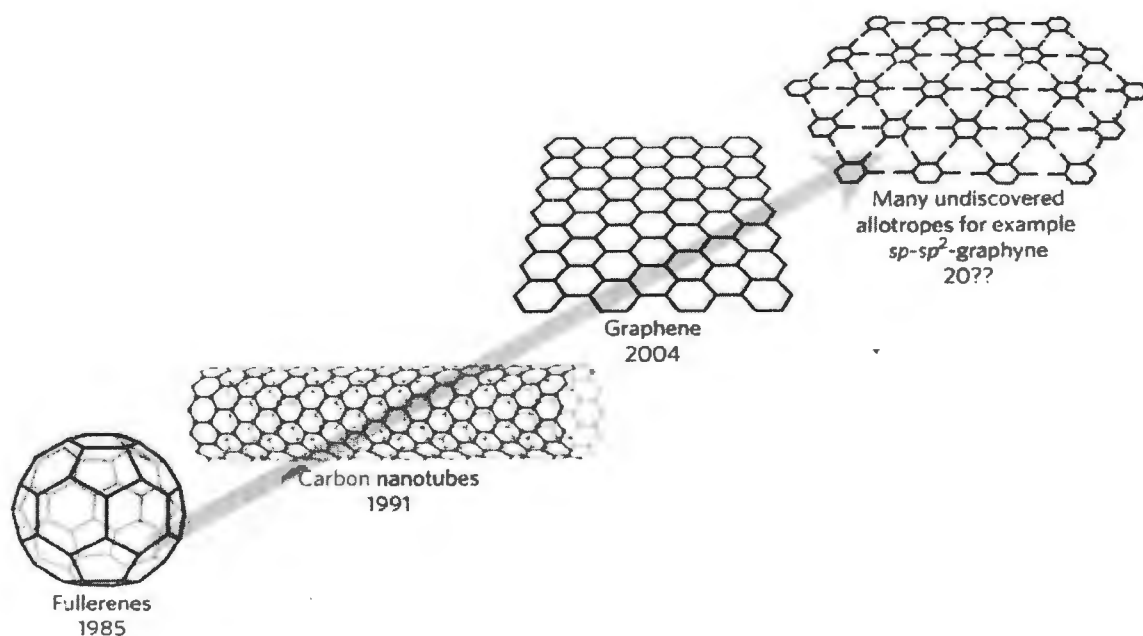
Figure 1.2: Some allotropes of carbon [4]

Carbon-based nanomaterials have attracted the scientific community because of its important role in nanoscience field [5].

Table1.1: The properties of graphene and other carbon allotropes [6].

Carbon allotropes	Graphite	Fullerene (C60)	Carbon nanotube	Graphene
Hybridized form	sp^2	Mainly sp^2	Mainly sp^2	sp^2
Crystal system	Hexagonal	Tetragonal	Icosahedral	Hexagonal
Dimension	Three	Zero	One	Two
Experimental specific surface area($m^2 g^{-1}$)	~10–20	80–90	~1300	~1500
Density (g cm^{-3})	2.09–2.23	1.72	>1	>1
Thermal conductivity (W $m^{-1} K^{-1}$)	1500–2000[a], 5–10[c]	0.4	3500	4840–5300
Optical properties	Uniaxial	Non-linear optical response	Structure dependent properties	97.7% of optical transmittance
Hardness	High	High	High	Highest (single layer)
Tenacity	Flexible non- elastic	Elastic	Flexible elastic	Flexible elastic
Electronic properties	Electrical conductor	Insulator	Metallic and semiconducting	Semimetal, zero-gap semiconductor
Electrical conductivity (S cm^{-1})	Anisotropic, 2–3*10^{4a}, 6^b	10^{-10}	Structure-dependent	2000

[a]**a-direction**
[b]**c-direction**

1.2.1 Fullerenes:

The discovery of a new molecular allotrope of carbon buckminsterfullerene was altered the world of carbon allotropes [7]. Fullerene is a cage-like carbon molecule which is 7 Å in diameter [8]. It is also known as C_{60} because it contain 60 carbon atoms. Fullerenes are zero dimensional objects because the carbon atoms are arranged spherically in it. By introducing pentagons in graphene we can get fullerene structure [9].
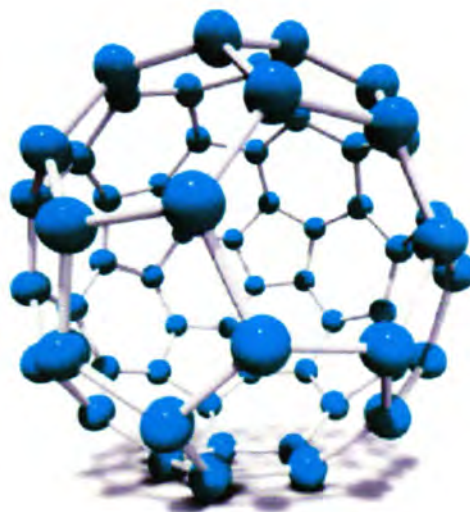
Figure 1.3: C_{60} or buckminsterfullerene [7]

1.2.2   Carbon nanotubes:

Carbon nanotubes discovered by Iijima in 1991 have attracted attention from scientists due to its unique physical, chemical, mechanical and thermal properties [10]. CNTs are one dimensional objects and consist of hexagons. CNTs can be obtained by rolling graphene sheets into cylindrical form and capped with half shape of fullerene structure.

SIDEWALL

CAP
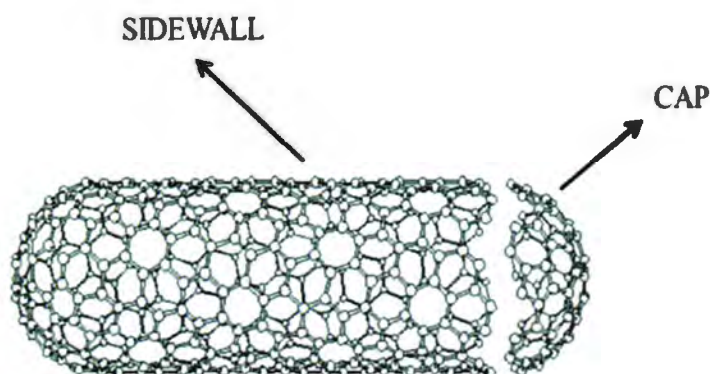
Figure 1.4: Carbon nanotubes [3].

Carbon nanotubes are of two type: (1) Single walled nanotubes (SWNTs) consists of single graphene sheet rolled to form a cylinder. SWNTs consist of two regions, side wall of tube and end cap of tube. (2) Multi walled nanotubes (MWNTs) made up of concentric multiple

graphene sheet rolled to form cylinders having interspacing of 0.34 nm and diameter of 10 to 20 nm [11].

1.2.3   Graphite:

Graphite is the longest known allotrope of carbon. It is made up of sp^2 hybridized carbon atom layers stacked in an ABAB manner in all three dimensions. Graphite consists of multiple layers of graphene. Bonding between carbon atoms in a single layer is covalent bonding and these parallel layers bound to each other through weak van der Waal force due to which this weak force, planes can slide over each other [12]. Distance between lattice planes is 3.37 Å and Distance between two hexagonal lattices in the same plane is 1.42 Å. Two covalent bonds make an angle of 120° with each other [8].
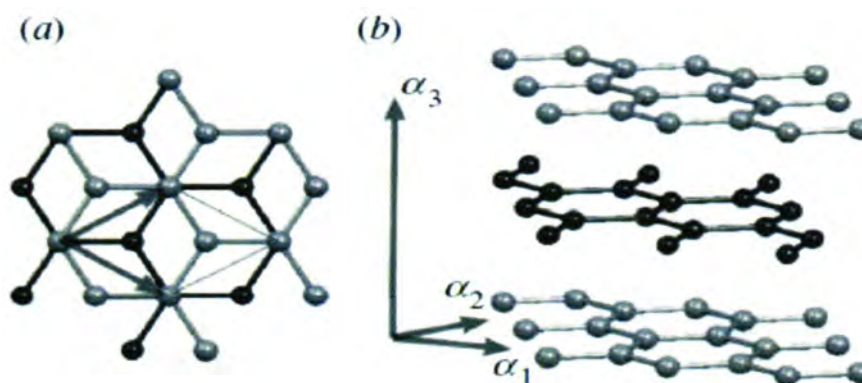
Figure 1.5: Graphite lattice **(a)** top and **(b)** side view [12]

Electrical and thermal conductivity of graphite is very high and it depends on its structure. Electrical resistivity of a single crystal graphite is from 4 to 6×10^{-5} Ohm-cm, just like a poor metal. But polycrystalline graphite has the crystal boundaries so its resistivity is much higher [13].

1.2.4   Graphite oxide:

Graphite oxide is derivative of graphite having large quantity of oxygen. It is a compound of oxygen, carbon and hydrogen. It contains epoxy, hydroxyl, carboxyl functional groups

[14]. It can prepare by oxidation of graphite with any oxidizing agent [15]. Graphite oxide structure has two different regions, the aromatic region with unoxidized benzene rings and the aliphatic six- membered rings [16]. It is made up of multiple layers of graphene oxide which is strongly hydrophilic. The inter-layer distance between the graphene oxide sheets increases reversibly with increasing humidity and it varies from 6 to 12 Å [17].

1.2.5 Graphene oxide:

Graphene oxide (GO) is oxygen-rich graphene in which atomic ratio of C/O is ~2. It is a graphene sheet with its basal plane decorated by oxygen-containing groups [18]. GO can synthesized by the oxidation of graphite and exfoliation of graphite oxide through ultrasonication. GO sheets are electrically insulating because the oxygenated functional groups (hydroxyl, carboxyl and epoxy groups) which reduce electron mobility so these functional group must remove to restore its conductivity [19]. GO is a promising precursor for a large-scale production of graphene [20].

1.2.6 Graphene:

In 2010 Andre K. Geim and Konstantin S. Novoselov both at the University of Manchester, get Nobel Prize in Physics because of their discovery of graphene in 2004. They produce, isolate, identify and characterize graphene nanosheets [21].

Graphene is 2D allotrope of carbon which consists of single layer of carbon atom arranged in a honeycomb lattice [22]. It is single layer of graphite in which carbon atoms are bonded with each other through covalent bonding. It is thinnest and strongest known material in the world [23]. Charge carriers in graphene show large intrinsic mobility and have zero effective mass. At room temperature, charge carriers can cover the distance of micrometers without scattering. Dirac equation can used to explain the transport of electron which investigate the relativistic quantum phenomenon in a benchtop experiment. It is zero band gap semiconductor or semimetal which means that graphene cannot be switched from conductive state to the non-conductive state [24].

Graphene is basic building block of other carbon-based material like fullerene, carbon nanotubes and graphite due to the fact that it can stretch and bend. Wrapped up form of graphene is called fullerene, when several graphene sheets are rolled up along a vertical

axis they give carbon nanotubes and by stacking the multiple layers of graphene on the top of each other, one can obtain the graphite structure [21]. Hence we can say that graphene is mother of all graphitic materials.

2-D (Grpahene)

0-D (fullerenes)   1-D (Nanotubes)   3-D (Grpahite)
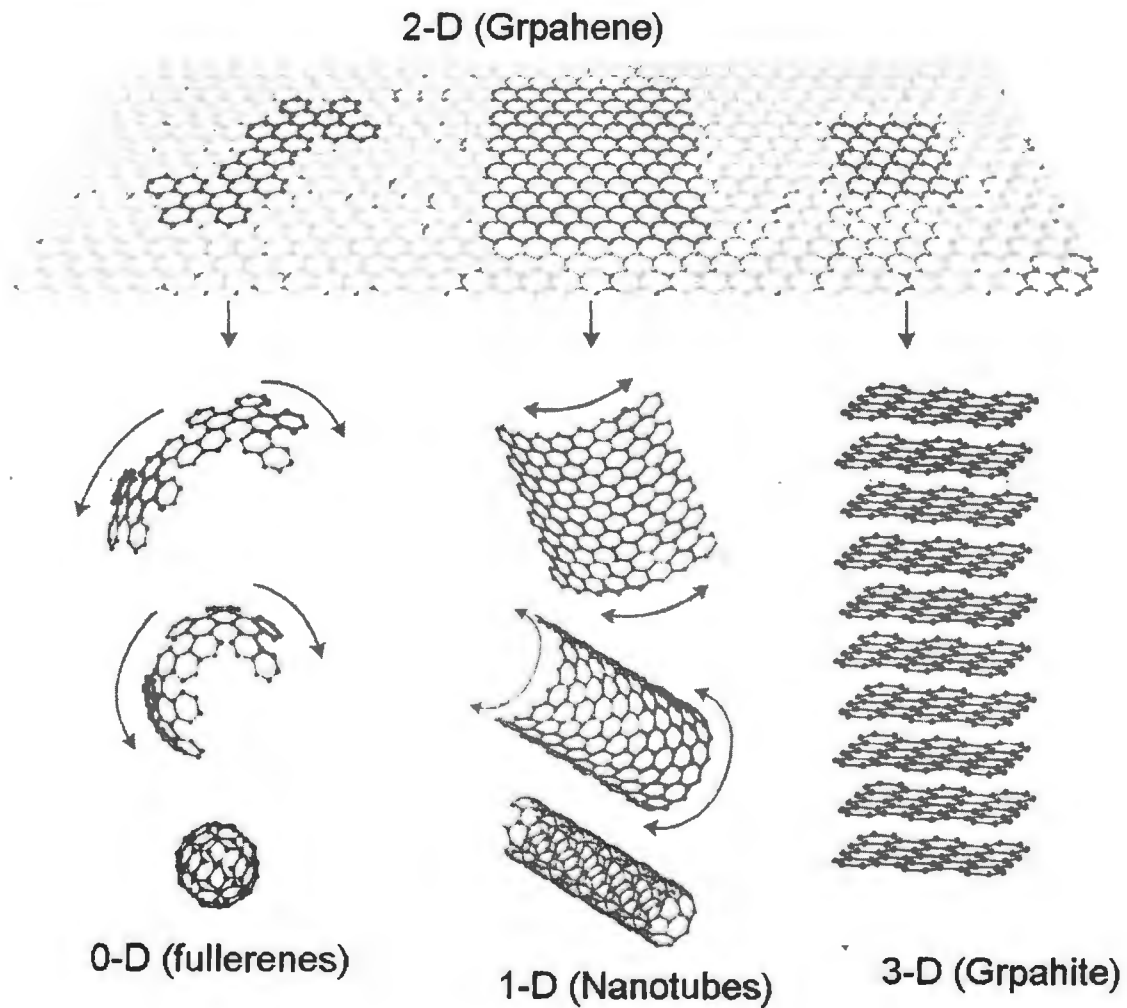
Figure 1.6: Graphene is basic building block of other allotropes of carbon [25]

Graphene gets tremendous attention of researchers because of its exceptional properties, such as large surface area (2,630 m^2 g^{-1}) [26], high values of Young's modulus (~1,100 GPa) [27], fracture strength (125 GPa) [27], good thermal conductivity (~5,000 W $m^{-1}K^{-1}$) [28], mobility of charge carriers (200,000 cm^2 V^{-1} s^{-1}) [29], excellent optical transparency

7

[30] and fascinating transport phenomena (quantum Hall effect and ambipolar electric field effect) [31]. Depending on these remarkable properties graphene and its derivatives have many applications in energy conversion and storage (e.g., fuel cells [32] and capacitors [33]), sensors [34], electro-catalysis [35], photo-catalysis [36], reinforced composites, biomedicine and electronic devices [37].
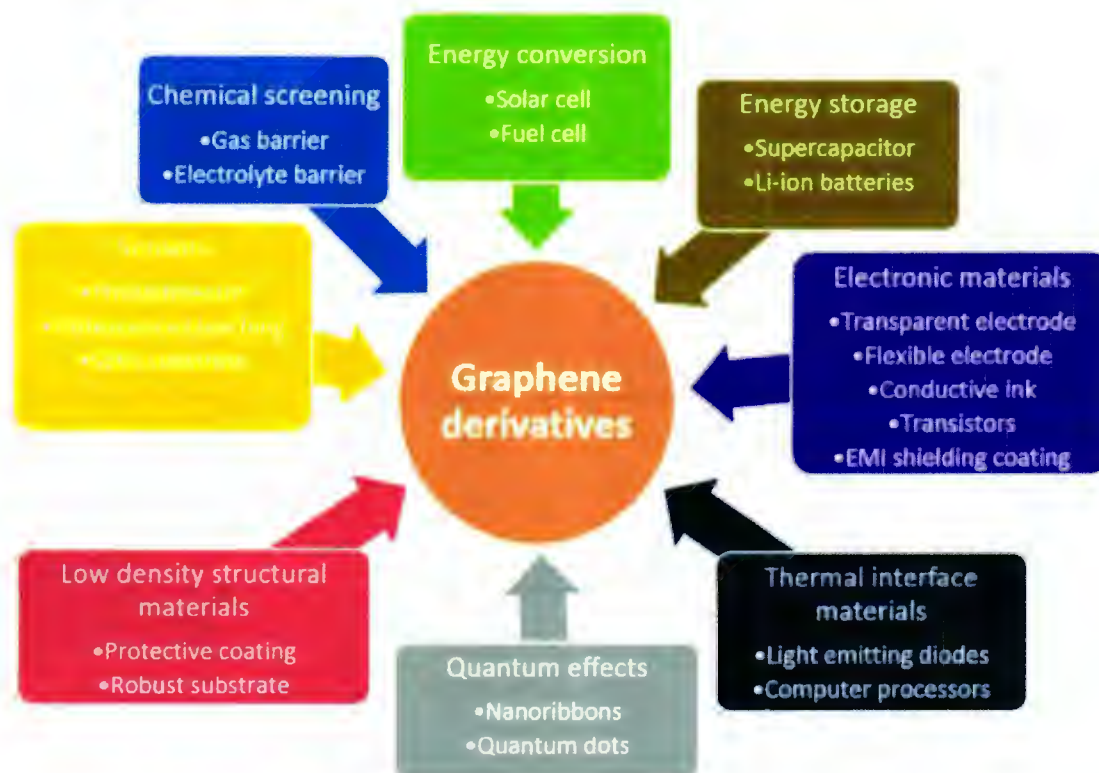
Figure 1.7:   Graphene derivatives has many applications in various fields [38].

1.3 Graphene structure:

1.3.1   Chemical bonding and sp^2 hybridization:

Graphene is a monolayer of carbon atoms. Carbon contains 6 electrons, the first 2 electrons present in the 1s orbital which are very close to the atomic nucleus so do not contribute in chemical bonding and have little effect on the physical properties of graphene. In the valence shell, hybridization occur between the s and p orbital's which results in sp^2 hybrid

covalent C-C bonds that make up graphene's honeycomb lattice. Hybridization means that, the one 2s orbital and two of the three 2p orbitals 'mix' together to produce three hybridized sp^2 orbitals. Each carbon atoms on honeycomb lattice form three strong covalent σ (bonding) and σ^* (antibonding) bonds with nearest neighbors [39]. In graphene, sigma bonds are responsible of most of binding energy and elastic properties [40]. The remaining 2p electrons in each carbon atom form π and π^* weaker covalent bonds contribute an important role in electronic properties of graphene sheet. Bonding orbitals are completely filled on the other hand antibonding orbitals are empty [21].
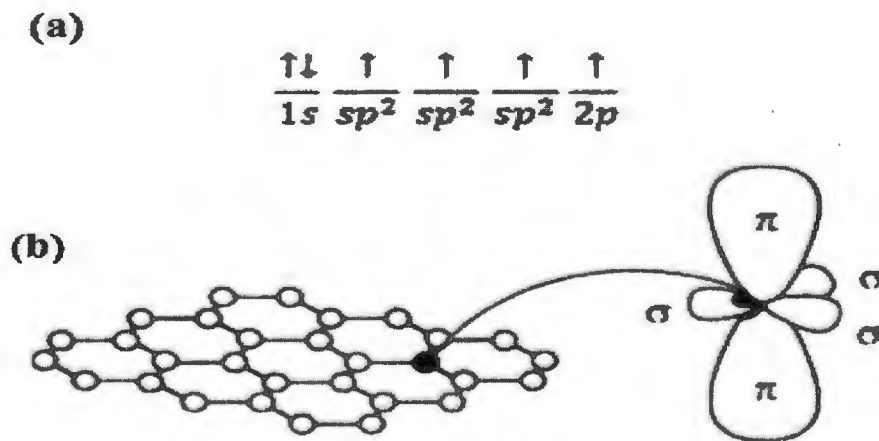
Figure 1.8: (a) Configuration of sp^2 bonding (b) Representation of π and σ bonds in real space [41]

1.3.2   Band Structure:

In graphene, σ bonds that give rise to honeycomb structure are responsible for the mechanical strength and the perpendicular π bonds contribute to its unusual band structure. Within brillouin zone, conduction and valence bands are in contact with each other at 6 points (k_x, k_y) i.e. $(0, -4\pi/3\sqrt{3}a)$, $(2\pi/3a, -2\pi/3\sqrt{3}a)$, $(2\pi/3a, 2\pi/3\sqrt{3}a)$, $(0, -4\pi/3\sqrt{3}a)$, $(-2\pi/3a, 2\pi/3\sqrt{3}a)$, $(-2\pi/3a, -2\pi/3\sqrt{3}a)$, where low energy dispersion relations are nearly linear and have zero effective mass [42]. By solving the Schrodinger equation, energy dispersion relation of π (bonding) and π^* (antibonding) bands can obtained [40].

$$E(k_x, k_y) = \pm\gamma\sqrt{1 + 4\cos\left(\frac{\sqrt{3}k_x a}{2}\right)\cos\left(\frac{k_y a}{2}\right) + 4\left[\cos\left(\frac{k_y a}{2}\right)\right]^2}$$

Equation 1.1

Electrons in these low energy regions are called 'Dirac fermions' that are governed by the Dirac equation. K and K' points where the bands meet each other are known as Dirac points [43].

To describe the band structure of graphene, orthogonal nearest-neighbor tight-binding approximation is followed. Which assume that electronic states can be represented by linear combination of $2p_z$ orbitals.
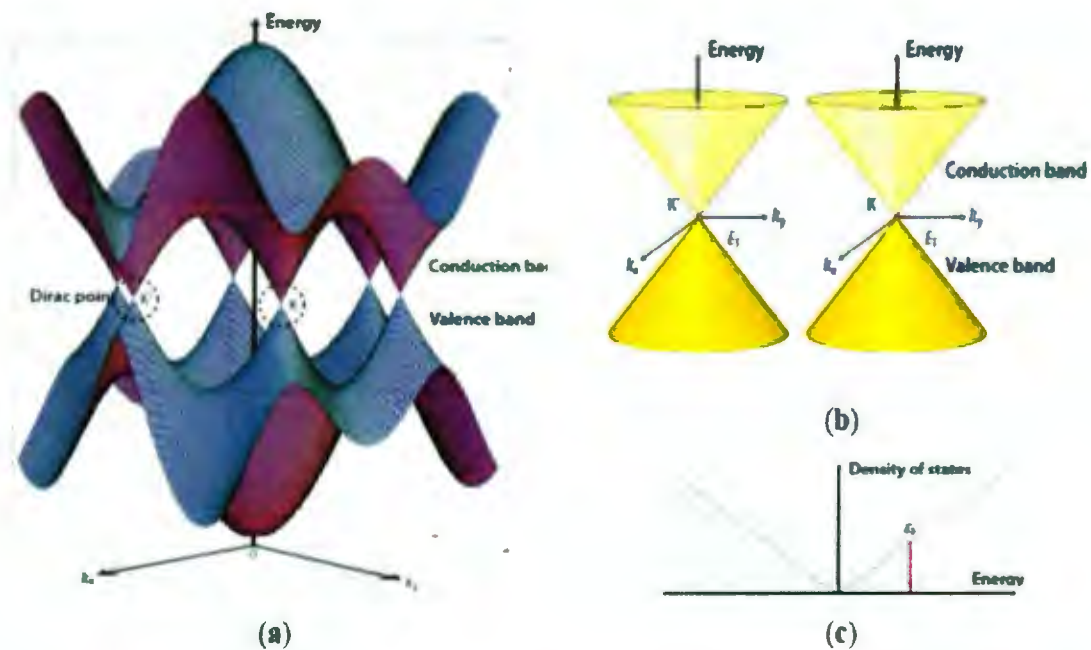
Figure 1.9: (a) conduction (π^*) and valence (π) band structure of graphene (orthogonal nearest-neighbor tight-binding approximation) **(b)** Conical energy spectrum near Dirac points K and K' **(c)** Density of state near Fermi level having Fermi energy E_f [44].

1.3.3 Lattice Structure:

The primitive cell of graphene consist of two non-equivalent atom basis, A and B, and these two sub lattices are translated from each other by a carbon–carbon distance a_{c-c} = 1.42Å [45]. Translation vectors a_1 and a_2 are given by

$$a_1 = \frac{a}{2}(3, \sqrt{3}), \quad a_2 = \frac{a}{2}(3, -\sqrt{3}) \qquad\qquad \text{Equation 1.2}$$

Reciprocal lattice vectors b_1 and b_2 are given by

$$b_1 = \frac{2\pi}{3a}(1, \sqrt{3}), \quad b_2 = \frac{2\pi}{3a}(1, -\sqrt{3}) \qquad\qquad \text{Equation 1.3}$$

And next nearest neighbors δ_1, δ_2, δ_3 are given by

$$\delta_1 = \frac{a}{2}(a, \sqrt{3}), \quad \delta_2 = \frac{a}{2}(1, -\sqrt{3}), \quad \delta_3 = -a(1,0) \qquad\qquad \text{Equation 1.4}$$
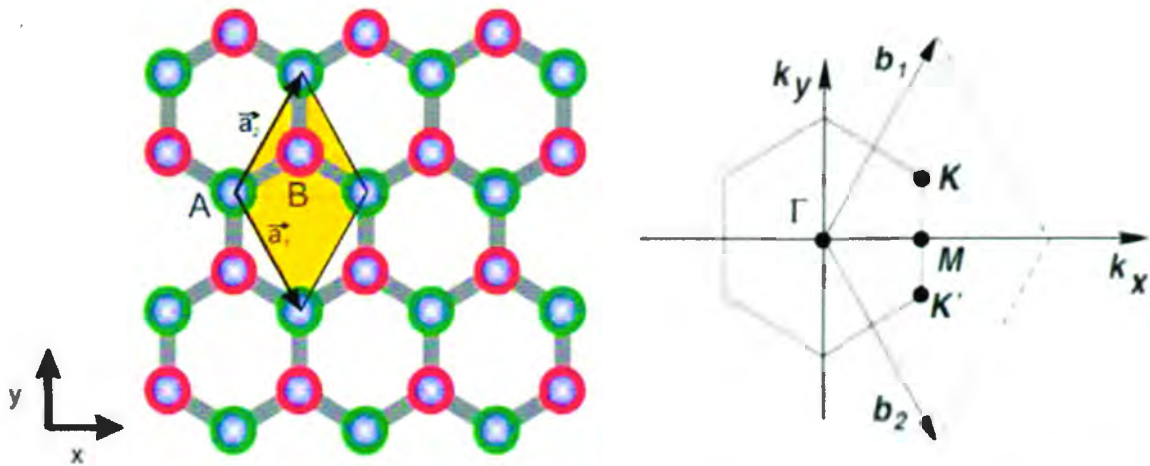
Figure 1.10: (a) Lattice structure of graphene in real space and its brillouin zone. **(b)** The Dirac cones are present at K and K' points [39].

First Brillouin zone for graphene is also hexagonal lattice. There are many high symmetry points in Brillouin zone: Γ point is the center point, the M point is at the midpoint of the hexagon, and K point is at the corner of the hexagon. First Brillouin zone contains six K points and six M points [46].

11

1.4 Properties of Graphene:

1.4.1 Mechanical Properties:

Graphene is one of the strongest material in the world because of its high breaking strength which is 200 times greater than steel. Its mechanical strength is 42 N/m and intrinsic mechanical strain is ~25%. In defect-free graphene, Young's modulus is ~1 TPa, Poisson's ratio is ~0.149 GPa and fracture strength is ~130 GPa [47]. Mechanical thickness can controlled by mechanical stress measurements performed on graphene sheets subjected to deformations induced by depositing different insulating capping layers [40]. Number of methods are successfully used to determine the mechanical properties, like numerical simulations (molecular dynamics), force displacement, force volume and nano-indentation atomic force microscopy (AFM). More interestingly ab initio, tight binding, molecular dynamics simulations, and semi empirical models are more successful models to estimate the Young's modulus and other mechanical properties of graphene [48]. When graphene is combine with the other carbon based materials such as carbon nanotubes (CNTs) or nanodiamonds, the strength, hardness and stiffness of composites increased up to 400%. Because of the high strength and ability to tune the mechanical properties, graphene has many potential applications such as fillers or reinforcements in medical implants, hydrogels and scaffolds used in tissue engineering [49].

1.4.2 Electrical Properties:

Electrical properties of graphene depend on spatial distribution of functional groups and structural defects [50]. Graphene is electrical conductor due to the presence of strong sp^2 C-C bonding. As in sp^2 bonding delocalized pi electrons are present which are responsible for graphene's conducting behavior. Another reason of high conductivity is the low defect density of crystal lattice of graphene. Electrical conductivity of defect free single layer graphene at room temperature is 104 S/cm. Electrical conductivity decreases when chemical modifications are done in graphene because in this process defects are introduce in the material. When impurities are added to graphene either adsorb on the surface or trap between graphene and substrate, the electron mobility of graphene is greatly affected [49].

1.4.3 Thermal Properties:

As thermal properties of all materials are related with the vibrational energy of atoms. Atoms in solid materials are constantly vibrating at high frequencies; these vibrations of adjacent atoms are coupled with each other by virtue of atomic bonding in such a way that travelling lattice waves are produced. These waves are elastic waves having short wavelength and higher frequencies which propagate through crystal at the velocity of sound. These elastic waves are also known as phonons. These phonons contribute in transport of energy during thermal conductance [51].

So the thermal conductivity of graphene can be described in terms of phonons known as diffusive conduction at high temperature and ballistic conduction at sufficiently low temperature. Phonon also contribute in specific heat of graphene [48]. Graphene exhibit excellent thermal properties because of its unique structure, strong sp^2 C-C bonding, low mass of carbon atoms and low defect density of crystal lattice. The thermal conductivity of defect-free single layer graphene is ~4500 to 5200W/mK which is significantly greater than that of graphene oxide (~2000W/mK), multiwall carbon nanotubes (~3000W/mK) and single wall carbon nanotubes (~3500 W/mK) [49]. Graphene has unique thermal properties including very high in-plane thermal conductivity and relatively low out-of-plane thermal conductivity. Thermal conductivity also depends on sample length because in sub-micron samples, in-plane thermal conductance G of graphene can reach a significant fraction of the theoretical ballistic limit [52]. Due to such high value of thermal conductivity, graphene play an important role in nanoelectronic devices [53].

1.4.4 Optical Properties:

Optical properties of any material depend on the nature of band gap. Graphene is zero band gap material because of sp^2 bonding [54]. As in sp^2 bonding delocalized electrons are present which are responsible for good conduction properties and this behavior attribute to the low band gap energy values nearly about 0.5ev.

Graphene gets lot of attention due to its excellent optical properties. Single layer of graphene transmit 97.7% of light incident on its surface so it is practically transparent material. It absorbs only 2.3% of incident light and this number can obtained by $\pi\, \alpha$, where

13

α is the fine structure constant [40]. Absorption of light increases with increase in the number of layers of graphene.

From infrared through the visible region, Dirac fermions has high-frequency conductivity equals to $\pi e^2/2h$. For normal incident light optical transmittance is given by $T = (1 +1/2\pi\alpha)^{-2}$ and reflectance is $R = 1/4\pi^2\alpha^2T$ (where $\alpha = 2\pi e^2/hc \approx 1/137$, e is the electron charge, c the speed of light, and h Planck's constant); the opacity is $(1 - T) \approx \pi \alpha \approx 2.3\%$ [48].

When light is absorbed by the graphene surface, electron-hole pairs are generated depending on carrier's density. These electron-hole pairs recombine in very short interval of time. But by applying external or internal field they can be separated to generate photocurrent. This ability of controlling recombination rate, makes graphene an important material in bio-imaging applications. It is also important in Magnetic Resonance Imaging (MRI) because of its High light transmittance, photoluminescence and high charge mobility [49].

1.4.5 Magnetic Properties:

Well known approach to modify the electronic structures, catalytic activity, and magnetic behaviors of nanoscale carbon surfaces is the adsorption or doping of foreign atoms. To understand these modifications in electronic and magnetic properties due to adsorption, it is necessary to study the interaction between ad atoms and the carbon nanosurface. This approach is also useful in fabrication of microelectronic devices and turning their transport properties [55].

Magnetic response can be induced in bulk graphene by introducing different types of point defects including vacancies and chemisorbed atoms [56]. The ideal sp^2 lattice structure is interrupted by point defect and new states are induced which are magnetic states. Magnetic properties in graphene can be induced by vacancies, substituting atoms, absorbed atoms, edge structures and edge states, finite size of graphene, electron–electron interaction, substrates, and strain [40].

In a weak magnetic field, the susceptibility of graphene can be calculated according to quasi-continuous Landau levels (LLs). The orbital angular momentum of electrons in a perpendicular magnetic field is obtained according to the electronic wave functions. It is found that the corresponding orbital magnetic moment is paramagnetic for negative LLs and diamagnetic for positive LLs. As a result, the susceptibility of carrier-undoped graphene is either diamagnetic or paramagnetic and magnetization decreases rapidly with increasing electrons or holes doping. This susceptibility is interesting and attempts have been done to find its origin [57]. Besides the transport and many other properties, magnetic properties of graphene are also very important in future applications [58].

1.5 Copper oxide (CuO):

Copper oxide also called cupric oxide is more attractive semiconductor material because of its unique chemical and physical properties including high electron communication features, high solar absorbency, high specific surface area, narrow band gap and high solar absorbency. In copper oxide, each copper atom is connected with the four neighbor oxygen atoms in an approximately square planar configuration [59]. Some properties of the cupric oxide are summarize in table 1.2.

Table 1.2: Properties of cupric oxide [59].

Property	*Value*
Structural: *a) stable crystal structure* *b) lattice constant*	a) monoclinic b) a = 4.68 Å, b = 3.42 Å, c = 5.13 Å
Electrical: *a) reversible capacity* *b) hole mobility*	a) 630 mA h g^{-1} b) 0.1-10 cm^2 / V s
Optical: *a) band gap* *b) refractive index*	a) 1.2 eV, direct b) 1.4

It is nontoxic, low cost material and present in abundance. Because of its unique electrical, optical and magnetic properties, it has been extensively used in photocatalysis, solar energy conversion, gas sensors, active electrode materials in lithium-ion battery, and as field emitter [60]. Cupric oxide based nanostructures and macrostructures such as nanorods, nanosheets, and nanodentrites and also honeycomb-like, urchin-like and dumbbell-like structures has received considerable attention because of their versatile properties and diverse applications. As industrial dyestuff is an organic compound which causes the discoloration of water and dangerous for aquatic life so removal of this color is important task for ensuring a safe and clean environment. During last ten years, advanced oxidation processes was used to degrade these dyes but these processes operate at high costs. To solve this problem, cupric oxide is one of the important material used as the environmental catalyst. Catalytic reaction depends on the structure of the material the exposed crystal planes. So structure and shape controlled synthesis of cupric oxide structure is important for desired catalytic applications [61].

1.6 Graphene in Photo-catalysis:

As environmental and energy problems are the biggest challenges for this century, so photo-catalytic nanomaterials get more and more attentions because of their applications in these fields. In basic photo-catalysis reaction, electron in valance band is excited to the conduction band by using source of light. This excited electron leaves behind a hole in valance band. This photo generated electron-hole pair on the surface of catalyst causes the redox reaction in the adsorbed molecules. As a result contaminating molecules are removed or reduced to less contaminating components before the annihilation of exciton [62].

Nanostructured semiconductor materials are important for photo-catalysis technology, but there are several problems associated with these materials such as fast electron–hole recombination rate and the mismatch between band gap energy and solar radiation spectrum, which limit their applications. To solve these problems, graphene can be used as supporting material with these semiconductor nanomaterials to improve the photo-catalytic activity [63]. Graphene has high surface area (2630 m^2 g^{-1}), excellent mechanical strength and aromatic-

rich structure. Due to these distinctive properties, graphene has extensive role as a catalyst or catalytic support for fuels and photo degradation of organics [64].

1.7 Copper oxide/Graphene in Photo-catalysis:

As cupric oxide (CuO) is the p-type direct band gap semiconductor having the bandwidth of 1.2 to 1.5eV [65]. Which possesses attractive photo-catalytic properties [66]. It has good applications in photo-catalysis, solar energy cell, hydrogen production, and anode material for lithium ion battery. But practical conversion efficiency of solar battery based on CuO is very small because of fast photo-generated electron-hole recombination and photo corrosion. To solve these problems, CuO is integrated on carbonaceous materials to improve the performance of photo-catalysts. So the combination of graphene and CuO plays an important role in photo-catalysis applications [63].

There are many reasons for the enhanced catalytic activity of the graphene/CuO nanocomposite. First, graphene can adsorb more dye molecules on the catalyst surfaces so that the catalyst and dye molecules can contact better. Second, in the composites material graphene can act as an electron acceptor allowing for the photo-excited electrons of semiconductor to be quickly transferred from the conduction band of semiconductor to graphene which is due to its two-dimensional π- conjugation structure. This property decreases the recombination rate of the photogenerated electron hole-pairs, which results in an enhanced photocatalytic activity of the composites [63].

Aims and Objectives of the Work

The aims of the present project are:

- To synthesize graphene nanosheets by using three different methods.
- To incorporate graphene oxide and all prepared samples of graphene with CuO and to measure the photo-catalytic activity of all synthesized nanocomposites by photo-degradation of MB.

- To characterize the structure and morphology of synthesized graphene nanosheets by different characterization techniques such as X-Ray Diffraction (XRD), Scanning Electron Microscopy (SEM), Energy Dispersive Spectroscopy (EDS), and Fourier Transform Infrared Spectroscopy (FTIR).

Chapter No. 2

Literature Review

Wang, Z-g, *et al*, [67] determined the green synthesis of reduced graphene oxide (RGO) and its electrical properties. Graphene oxide (GO) was synthesized by modified Hummer's method. Reduction of graphene oxide was done by two different methods, ethanol-thermal reaction and hydrothermal reaction. Products were characterized by XRD, TEM and XPS. Results study reveals that ethanol is more effective reducing agent for reduction of GO than the supercritical water under solvothermal condition. Which causes that RGO reduced by ethanol has lower oxygen contents but higher electrical conductivity than RGO synthesized by hydrothermal reaction.

Yuan, W, *et al*, [68] determined the green synthesis of graphene nanosheets by using glucose for reduction of exfoliated graphite oxide. Hummer's method was adopted for the fabrication of graphite oxide and exfoliation was done. Hydrogen storage properties of as-synthesized material was studied. Structural and morphology of resultant material was characterized by XRD, SEM, FTIR, TEM, AFM and Raman spectroscopy. XRD and FTIR results confirm the reduction of graphene oxide and Raman spectroscopy tell us about the changes occur structure during reduction. Morphology was given by SEM and TEM results which revealed that graphene has transparent sheets like morphology. AFM indicated that graphene sheets have thickness approximately~1.3nm and samples contain mostly single-layer graphene and multi-layered graphene at somewhere. BET measurements give the specific area~1205.8m2g-1 and N_2 adsorption-desorption isotherms exhibit type-I curve and give hysteresis loop which could be attributed to the porous structure of the graphene sheets i.e. presence of pores between parallel layers of the graphene. Hydrogen adsorption property was observed by the magnetic suspension balance gravimetric analyzer. Hydrogen storage capacity has direct relation with the H_2 pressure and reversely related to temperature. Graphene has hydrogen storage capacities~1.2 wt. % at 328K and 2.7 wt. % at 298 K under 25 bar. Thus graphene sheets showed the outstanding properties for the application of hydrogen storage.

Wu, T, *et al*, [69] described the new chemical route to synthesized reduced graphene oxide by using Copper nanoparticles. Cu nanoparticles were used as reducing agent for reduction of graphene oxide. Reduction of GO was confirmed by XRD, UV-Visible spectroscopy, TEM, XPS, TGA and Raman spectroscopy. Cu powder was also used to reduce GO under the same conditions

but Cu nanoparticles has high reduction ability. Reduction of GO results in the oxidation of Cu nanoparticles and Cu_2O supported on reduced GO was formed. The final product Cu_2O/RGO has high catalytic ability. Catalytic activity of Cu_2O/RGO was tested by studying the catalytic degradation of dye pollutant methylene blue (MB).

Wang, K, *et al*, [70] developed a green, appropriate and economical approach to produce graphene field emitters. Hummer's method was followed for the preparation of graphene oxide. GO was reduced by using hydrazine (HR-GS) and another method was the reduction in microwave synthesis system (MW-GS) and then different samples were prepared for field emission test. XRD results of GO contain a wide peak at 10° was due to the damage of lattice of graphite. This peak was nearly removed after reduction by hydrazine and microwave. Which clearly shows that multilayered graphite structure transformed in to single layer or several layers graphene. In DRS, absorption peak of the HR-GS dispersion shifted from 231nm to 265nm, on the other hand the absorption peak of MW-GS shifted to 260nm. I–V characteristics of both graphene samples shows that MW-GS has much higher value of field emission current than that of HR-GS at the same voltage and HR-GS has smooth I–V curve than MW-GS. It shows that in MW-GS emission current become more stable. Results of XRD, TEM and UV-visible DRS proved that graphene produced by both methods has same reduction level but field emission results reveal that microwave synthesis is more suitable to synthesize graphene films for field emitters.

Sim, H, S, *et al*, [22] described repeated supercritical carbon dioxide ($scCO_2$) process to prepare graphene nanosheets (GNs). Thickness of graphene sheets further decreases by repeating $scCO_2$ process. So there is a possibility to prepare thickness-controlled GNs by controlling numbers of $scCO_2$ process. GNs were characterized by SEM and AFM. SEM results show that particle size of graphite was 5-10 µm and its layers was densely stacked to each other. After $scCO_2$ the lateral size of GNs was about 0.3–0.5 µm and it was transparent sheets unlike graphite, which shows that thickness of GNs decreases by $scCO_2$. These thinner GNs show higher conductivity than chemically reduced GO because there is no oxidation and reduction process.

Orofeo, Cn *et al*, [71] synthesized the large area, homogenous, single layer graphene on cobalt (Co) and nickel (Ni). Large area, single layer graphene was obtained after sputtered amorphous carbon deposited on Co/sapphire or Ni/sapphire substrate and then vacuum annealing. Area of obtained graphene was 100mm^2 which depends on the substrate and vacuum chamber size. Resultant graphene product was characterized by XRD, TEM, AFM and Raman spectroscopy.

Graphene films were grown at different cooling rates, there was no noticeable difference in homogeneity of films produced for all cooling rates. So homogeneity of graphene was independent of cooling rate. The transport properties of graphene were investigated by making field effect transistors based on graphene and by measuring the resistant of sheets using the van der Pauw method. The mobility of carriers in graphene was ~ 1050cm^2 / (V.s) and Dirac point were shifted to the~+48V exhibiting p-type behavior. Which is due to the adsorption of oxygen and water molecules or unintentional doping of graphene that stop the n-type conduction.

Lia, X, *et al*, [72] described a method to grow graphene on metal substrate by chemical vapor deposition. Graphene was grown on Cu foil and then transferred to the Si_2O/Si substrate by wet chemical etching of Cu. Final transferred graphene films were characterized by SEM, TEM, UV-VIS and Raman spectroscopy, and four-point probe electrical measurements. TEM was performed to find no of layers and crystalline quality of graphene. No of layers were determined by counting no of fringes at edge of samples. Result shows that film has graphite like hexagonal structure and film consists of 2 to3 no of layers. Crystal quality was also determined by Raman spectroscopy. Results described that graphene transferred film has low defects determined by the absence of "D" band at 1350 cm-1 in the Raman spectrum. Graphene films grown on Cu substrate show high transmittance and low resistance, these unique properties make them important in optoelectronic applications. This method can be used for the large scale production of graphene thus compatible with the sizes required in semiconductor industry.

Krasnenko, V, *et al*, [73] theoretically studied the modification in structural ant electronic properties of graphene by the adsorption of benzene molecules. Before this, literature on the adsorption of benzene on graphene indicate that benzene molecules were bonded to graphene through weak van der Waals forces and distance between graphene sheet and benzene molecule is 3.40 Å   . In this study, it was found that depending on the separation of graphene sheet and benzene, two opposite situation can be realized. (1) Benzene and graphene sheet bonded with each other through strong covalent bonds when distance between graphene layer and benzene was ~1.60 Å. Due to this short distance, carbon atoms of benzene move towards graphene and hydrogen atoms move in different directions which break the benzene planar structure. Aromatic rings of both materials move towards each other. There was remarkable change in geometric configuration and electronic properties, zero band gap graphene was transformed in to semiconductor material with band gap of 0.8V. In addition to this slight negative charge appear on the carbon atoms

21

because of the re-distribution of electron density. (2) One week van der Waals interaction may present between graphene and benzene at larger distance ~ 3.3Å. In this situation both graphene and benzene maintain their planar structure and band gap disappear which results in the enhanced metallic behavior.

Zhao, J, et al, [74] produced the porous graphene films by electrospraying on Si_2O coated Si substrate and studied its optical and magnetic properties. Prepared graphene films were characterized by FESEM, TEM, SAED, AFM and UV-Vis spectroscopy. XPS, infrared spectroscopy and Raman spectroscopy for further confirmation of porous graphene films formation. TEM and SAED results demonstrate the formation of few-layer graphene. AFM result gives the thickness of graphene and shows that graphene consists of approximately 3 layers. Morphology of porous graphene can revealed by FESEM. It explain that porous graphene has large surface area and promising electrical properties showing potential applications in gas sensor, lithium battery and catalyst. In addition porous graphene exhibit good adhesion to the substrate which leads to the fabrication of high-performance electronic and magnetic devices based on graphene. Reflection spectrum indicates that light absorption plays dominant roles at 375 and 635 nm. Two interesting features were, the logarithmic increase of the resistance and negative MR at low temperature. These characteristics were induced by the weak localization effect for 2D electronic system.

Wang, Y, et al, [75] described an electrochemical method of selective detection of dopamine based on graphene modified electrode. Graphene was chemically synthesized by Hummers method then graphene-modified electrode were fabricated for dopamine detection. Synthesized graphene was characterized by XRD and TEM. Results of XRD and TEM indicate the successful synthesis of graphene sheets. Dopamine is a neurotransmitter play an important role in the function of the central nervous, renal and hormonal systems. As ascorbic acid is always present with dopamine in organisms and have shares similar oxidation potential in electrochemical detection. To solve this problem, graphene based electrode were synthesized for selective detection of dopamine by completely eliminating the ascorbic acid. Very strong π–π stacking interaction between dopamine and graphene surface may speed up the electron transfer on the other hand it weaken the oxidation of ascorbic acid on the graphene based electrode. By comparison with the multi-walled carbon nanotubes-modified electrode it was confirmed that, graphene shows the good performance and better for the electrode materials. These unique electrochemical responses of graphene were due

22

to the two dimensional planar geometric structure and special electronic properties of graphene. This response to dopamine indicates that graphene can exhibit potential performances for other biological molecules proteins, nucleic acids, and enzymes.

Wang, Y-X, *et al*, [76] studied the electrochemical properties of reduce graphene oxide for the sodium ion storage. As sodium is abundant and low cost material so sodium ion battery is most favorable for sustainable energy storage. Graphene oxide was prepared by conventional modified Hummers method and then graphene nanosheets were obtained from prepared graphene oxide by giving heat treatment for 10 h in nitrogen atmosphere. Then electrochemical properties were examined in an electrolyte consisting of 1 M $NaClO_4$ in propylene carbonate. Fabricated reduced graphene oxide was characterized by XRD, TEM, FESEM, XPS, AFM and Raman spectroscopy and electrochemical properties were tested by performing Cyclic voltammetry. XRD results indicate the successful reduction of graphene oxide to graphene. Experimental results show that graphene possess disordered layered structured with the large amount of free space between these layers which facilitates the sodium ion storage. Prepared anodes based on reduced graphene oxide shows excellent sodium ion storage at room temperature with excellent capacity and long-term cycling stability at high current densities.

Anand, K, *et al*, [77] introduced an in situ method to prepare the nanocomposite of graphene/zinc oxide by reducing zinc acetate and graphene oxide during refluxing and this composite was used for hydrogen sensing purpose. Morphology and structure of synthesized material was studied by XRD, FESEM, EDX and FTIR. These results indicate the successful reduction of graphene oxide and synthesis of graphene/zinc oxide composite. For sensing purpose, a thick film of powdered nanocomposite was fabricated on alumina substrate. Sensing results exhibit that 1.2 wt% graphene/ZnO composite show the maximum hydrogen sensing response among all other concentration at operable temperature of 150 °C. Composite with other than 1.2 wt% concentration and pure ZnO exhibit less sensing response towards hydrogen gas. Addition of graphene in ZnO resulted in the decrease in operable temperature and increase in sensing response. Results also revealed that conductivity of pure ZnO and composite increases with increase in temperature which confirms the semiconductor nature of these materials. Conductivity of composite also increases with the concentration of graphene because of high conductivity of graphene and interaction between p-type graphene and n-type zinc oxide.

Li, F, *et al*, [78] fabricated the multilayer films of graphene/Ag/Al-doped zinc oxide (AZO) for flexible organic light emitting diodes (FOLED). Graphene was synthesized by chemical vapor deposition on cupper sheet then transferred to the transparent polyethylene terephthalate (PET) substrate and after this Ag and AZO were also deposited on it to obtained multilayer films. Synthesized films were used as anode in FOLED with 11nm thick Ag layer and 50nm thick AZO layer. Optical and electrical properties prepared films were studied which revealed that multilayer films can maintain high conductivity and transmittance without obvious degradation during bending cycle test and also has good light-emitting stability. Thus graphene/Ag/AZO has promising applications in flexible optoelectronics field.

Cao, J, *et al*, [79] prepared the asymmetric supercapacitor based on MnO_2 and graphene electrodes. MnO_2 nanoparticles were synthesized by reduction of $KMnO_4$ and graphene by reducing graphene oxide. Structure and morphology of materials was observed by XRD and SEM, while XPS gives the confirmation of reduction of the materials. In supercapacitor MnO_2 worked as positive electrode and graphene as negative electrode. This type of asymmetric supercapacitor can work at very high reversible cell voltage of 2V. The asymmetric cell has energy density of 25.2Wh kg-1 at power density of 100Wkg-1. On the other hand, symmetric supercapacitor based on MnO_2/MnO_2 shows the energy density of 4.9Wh kg-1 and based on graphene /graphene shows the energy density of 3.6Wh kg-1. Thus asymmetric supercapacitor has much higher energy density than symmetric supercapacitor and asymmetric system also has 96% capacitance retention after 500 cycles. Results reveal that asymmetric supercapacitors are more efficient for practical applications.

Cheng, K, *et al*, [80] created the pores in graphene nanosheets by treating graphene oxide with acid. Created pores were investigated by FE-TEM and AFM. Then reduced porous graphene oxide (rPGO) supported Pt (Pt/rPGO) catalyst was prepared and H2 heat treatment was conducted to improve the stability of the catalyst. Electrochemical impedance spectroscopy (EIS) analysis revealed that the porous GNS supported Pt catalyst is more efficient to reduce the mass diffusion resistance and also enhanced the oxygen reduction reaction activity. In addition to this improved the electrochemical surface area compared with the raw graphene nanosheet supported Pt catalyst can be obtained by creating pores in graphene nanosheets. Thus porous graphene based catalyst has enhanced electrochemical activities in proton exchange membrane fuel cells and has potential applications in other fields.

Qian, Y, *et al*, [81] prepared the Cuprous Oxide (Cu_2O) nanoparticles/Graphene hybrid with better electro-catalytic sensing towards glucose. Graphene oxide was prepared by conventional Hummers method. Then simple and effective approach was adopted for the in situ decoration of Cu_2O nanoparticles on graphene nanosheets. Sodium citrate was used as reducing agent and stabilizer for the first time. Microstructure and morphology was studied by XRD, AFM, EDX, TEM, and electrochemical technique. Results indicate that crystal Cu_2O nanoparticles has excellent dispersion with the uniform size distribution which was obtained via using sodium citrate. In addition to this prepared Cuprous Oxide (Cu_2O) nanoparticles/Graphene hybrid shows the better electrochemical responses towards glucose than individual chemically reduced graphene oxide or Cu_2O in alkaline media. Thus Cuprous Oxide (Cu_2O) nanoparticles/Graphene hybrid has potential applications as an advanced electrode material in electrochemical sensing and other electro-catalytic applications.

Abulizi, A, *et al*, [82] described the one-step fabrication of Cu_2O/reduced graphene oxide hybrid through simple sonochemical route without any surfactants or templates. Graphene oxide was prepared by conventional Hummers method then Cu_2O/reduced graphene hybrid was fabricated through simple sonochemical route. The morphology and structure of the composite was investigated by SEM, TEM, XRD, FTIR, XPS and Raman spectroscopy. Results revealed that the Cu_2O spheres were well distributed on graphene surface with an average size of 200 nm. In composite, morphology and composition can be controlled by simply controlling the molar ratio of reactants under ultrasonic irradiation. Prepared composites were used as photo-catalyst for degradation of methyl orange in photo-catalyst reaction. The as-prepared Cu_2O/ reduced graphene oxide hybrid shows excellent stability and photo-catalytic response in the photo-degradation of methyl orange in the presence of UV-light as compared to the pure Cu_2O. So it has good applications for water treatment, sensors, and energy storage. The enhanced photo-catalytic degradation efficiency was due to reduced graphene oxide because reduced graphene oxide not only acts as a charge acceptor to support the separation and transfer of carriers generated by light but also stabilize the Cu_2O spheres and adsorb methyl orange molecules in the aqueous solution. Thus, the combination of the 3D structure with the nanospheres having large surface areas and the highly dispersed can be a promising material for future nanotechnology.

Yanga, Y, J *et al*, [83] synthesized Copper sulfide/reduced graphene oxide nanocomposites used as the hydrogen peroxide (H_2O_2) and hydrazine sensor. Graphene oxide was prepared by modified

Hummers method and Copper sulfide /reduced graphene oxide nanocomposites were synthesized by hydrothermal method. Morphological and structural properties were characterized XRD, SEM, TEM and electro-catalytic performances were studied by cyclic voltammetry and amperometry. The results showed that aggregations in graphene nanosheets were reduced after its modifications with copper sulfate. Electrochemical characterization indicated that composites give excellent electro-catalytic performances towards the detection of both hydrogen per oxide and hydrazine. The sensor exhibited good reproducibility, selectivity, fast response, good stability and high sensitivity in the case of both analytes.

Rong, X, et al, [84] prepared the TiO_2/graphene nanocomposites as a photo-catalyst under the visible light illumination. Graphene oxide was synthesized from natural graphite by Hummers method and TiO_2/graphene hybrids were prepared by hydrothermal method. Structure, morphology and chemical composition was explained by XRD, SEM, TEM, FTIR, EDX, XPS, SEAD and Raman spectroscopy. XPS results revealed that TiO_2 interacts with graphene. TiO_2/graphene nanocomposites were used for degradation of methylene blue (MB) in the presence of visible light. As-prepared composites with 20% graphene oxide contents exhibited the excellent photo-catalytic response by giving the 98.8% degradation of MB in 100 min. High photo-catalytic performance was obtained by increasing the amount of graphene. The reason is that, band gap reduces with the increase in graphene contents. For which graphene slow down the recombination rate of electron and hole, enhanced the charge transfer rate of electrons, and also increase surface-adsorption of MB molecules through $\pi-\pi$ interactions. Thus TiO_2/graphene photo-catalyst is a promising material for treatment of industrial effluents waste water that contains MB.

Zhou, X, et al, [85] first time prepared the reduced graphene oxide (RGO)/copper phthalocyanine (CuPc) hybrid material and studied its sensing properties towards NH_3. Firstly graphene oxide was prepared by modified Hummers method and RGO/CuPc hybrid was synthesized by using hydrazine as reducing agent in the presence of CuPc. Synthesized hybrid material was characterized FTIR, TEM, SEM, XPS, Raman and UV-vis spectroscopy. In results, red shifted UV-vis peaks, binding energy shift in XPS, and G band shift in Raman spectroscopy determined the $\pi-\pi$ stacking interactions between reduced graphene oxide and copper phthalocyanine and also electron transfer interaction from copper phthalocyanine to the reduced graphene oxide. As-prepared hybrid based sensor showed much higher sensitivity towards NH_3 and recovery time was 10 times faster than the sensor based on reduced graphene oxide alone. During the sensing process,

copper phthalocyanine was acts as favorable active sites for NH_3 adsorption and after adsorption charge quickly transfer from NH_3 to CuPc. Sensor also exhibit good selectivity so important for selective detection of NH_3 at room temperature. Thus reduced graphene oxide/copper phthalocyanine hybrid is promising material for gas sensing and optical gas sensing application with the advantages of low cost, low power and portable properties.

Li, Q, *et al*, [36] determined a microwave-assisted synthesis of silver (Ag)/reduced graphene oxide (RGO) nanocomposite and studied its photo-catalytic properties in presence of visible light. Graphene oxide was prepared by Hummers method, then nanocomposite was synthesized under micro-wave irradiation and using ethanol for reduction of graphene oxide. Synthesized hybrid material was characterized by SEM, TEM, XRD, FTIR, and XPS. SEM and TEM results indicated that silver nanoparticles attached to the reduced graphene oxide sheets has average size of 5 to 10 nm. XRD showed that Ag nanoparticles has face-centered cubic structure and also confirmed the strong interaction of Ag nanoparticles with reduced graphene oxide. FTIR and XPS results determined the reduction of graphene oxide into reduced graphene oxide in hybrid material. The photo-catalytic performance was checked by the decomposition of Rhodamine B (RhB) under visible light. Results indicated that as-prepared Ag/RGO hybrid exhibits the enhanced photo-catalytic degradation of RhB than that of pure Ag nanoparticles. Thus Ag/RGO based nanocomposite is potential application for environmental purification.

Chapter No. 3

Synthesis Method

3.1 Equipment:

Following equipment are used in synthesis

- Drying oven
- Heating plate
- Sonication bath
- Magnetic stirrer
- Centrifuge machine
- Microwave synthesis system
- Photo-catalytic Reactor assembly

3.2 Chemicals Used in Synthesis:

Table 3.1: Chemicals used in the synthesis.

Chemicals	Formulas	Grades
Natural graphite	C	A.R
Sodium Nitrate	$NaNo_3$	A.R
Sulfuric Acid	H_2SO_4	A.R
Potassium Permanganate	$KMnO_4$	A.R
Hydrogen Peroxide	H_2O_2	A.R
Hydrochloric Acid	HCl	A.R
Ammonium Hydroxide	NH_4OH	A.R
Copper Oxide	CuO	A.R
Deionized Water	H_2O	A.R
Toluene	C_7H_8	A.R

3.3 Synthesis of Graphene Sheets by Oxidation and Reduction Method:

3.3.1 Preparation of Graphite Oxide:

Firstly, Graphite oxide (GtO) is synthesized by making some modifications in conventional Hummers method [86]. 23ml of sulfuric acid (H_2SO_4) is placed into beaker in an ice bath to set the operational temperature at 0°C. 1.5g of natural graphite is added and stirred for 5min to achieve the dispersion of graphite powder in sulfuric acid. Then 0.5g of sodium nitrate ($NaNo_3$) is placed into the dispersion and give the stirring of 30min to homogenize it. Solution is removed from ice bath and 3g of potassium permanganate ($KMnO_4$) is slowly added with very slow stirring. Solution was allowed to react at 35°C for another 1h. At this stage solution become pasty with brown color. Then 40ml of deionized water is gradually added to the mixture and stirred for 30min. Another addition of 100ml of water is done for further dilution and kept solution at 70°C for 1h. Reaction is terminated with addition of deionized water and 30ml of hydrogen per oxide (H_2O_2) to reduce the residual $KMnO_4$ and MnO_2 to soluble $MnSO_4$. Due to this treatment solution become bubbly and its color changed to brilliant yellow which indicating that graphite is oxidized in to graphite oxide. Graphite oxide particles are separated from the solution and washed with the 5% HCl solution to remove metal ions. At the end washed with the deionized water to remove unwanted HCl. Final product is dried at 60°C to obtain the graphite oxide powder (GtO).

3.3.2 Exfoliation of Graphite Oxide:

Exfoliation of graphite oxide (GtO) is done to convert the graphite oxide in graphene oxide (GO). For exfoliation, re-dispersed the graphite oxide powder into deionized water to obtain yellow-brown dispersion and then this solution is ultra-sonicated for 2h. Graphene oxide (GO) powder is obtained after centrifugation and drying at 60°C.

3.3.3   Reduction of Graphene Oxide:

Graphene sheets are prepared by reduction of graphene oxide (GO) in following two different ways.

3.3.3.1 Preparation of Graphene Sheets by Using Ammonia as Reducing Agent (GA):

25ml of ammonia is mixed into the 25ml of deionized water in beaker and stir together for 30min at 25°C to get homogenized ammonia solution. 1g of synthesized graphene oxide (GO) is added into ammonia water while stirring. Then directly placed this solution into the microwave synthesis system for 90min by setting the microwave oven at low power. Reduced graphene sheets are settled at the bottom of the beaker and can easily be separated after cooled down the solution at room temperature. Final graphene sheets are obtained after washing with deionized water and drying at 60°C. This graphene product is labeled as GA.

3.3.3.2 Preparation of Graphene Sheets by Using Plant Extract as Reducing Agent (GP):

1g of as prepared graphene oxide is suspended into 90ml of deionized water to obtain brown dispersion and stir until homogenize. Then 10ml of plant extract is gradually added into the solution while stirring. Dispersion is directly placed into the microwave synthesis system for 120min by setting microwave oven at low power. Graphene product is settled at the bottom of the solution and can easily be separated after cooled down the solution at room temperature. Final graphene sheets are obtained after washing three times with deionized water and product is dried at 60°C. This graphene product is labeled as GP.

Graphite oxide

Graphite

Oxidation

By using KMnO₄
and NaNO₃

By ultra-sonication in   **Exfoliation**
water

graphene sheet   **Graphene oxide (GO)**

Reduction
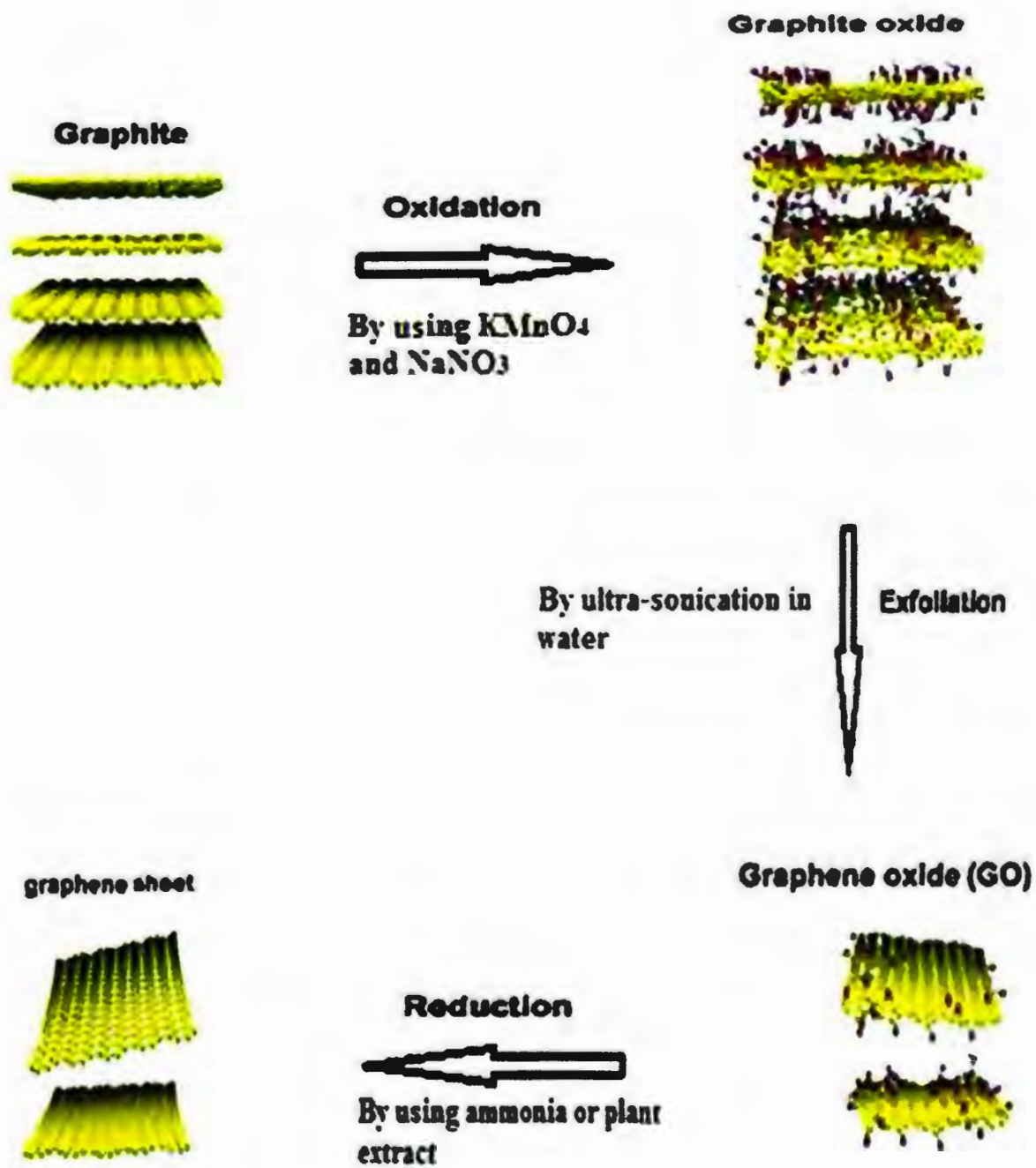
By using ammonia or plant
extract

Figure 3.1: Preparation route of graphene nanosheets.

3.4 Microwave Assisted Synthesis of Graphene Sheets (GM):

Graphene sheets are synthesized by making some modifications in method reported in literature [87]. Firstly, ammonia (50%) and deionized water (50%) are mixed and stirred together at 25°C for 30min to get homogenous aqueous ammonia. 2g of expandable graphite is added in ammonia water and dispersion is homogenized by giving the stirring of 24h at 25°C. Set the microwave oven at low power and put this solution directly into the microwave synthesis system for 90min. Graphene sheets are achieved in the form of suspension in aqueous phase above the solid residual of expended graphite. Graphene sheets are extracted from the suspension by a toluene-ammonia system. For extraction, 50% toluene and 50% ammonia are mixed together to obtain 100ml toluene-ammonia solution. Suspension of graphene sheets is then added to the toluene-ammonia solution. Transfer this solution to the separating funnel, two layers are formed and graphene sheets are dissolved in the lower layer. Graphene is separated easily from lower layer. Finally, it is dried at 60°C and labeled as GM.

3.5 Modifications with Cupric Oxide (CuO) nanoparticles:

Firstly, 10ml of ethanol is added into the 10ml of deionized water while stirring in the beaker. CuO nanoparticles (0.01g) are then dispersed in above solution and kept at stirring for 20min. 0.1g of as-prepared graphene oxide (GO) is added and stirred for 20min to obtain well dispersed and homogeneous solution. At the end, particles are separated from the solution when settled at the bottom. Final graphene oxide/copper oxide (GO/CuO) nanocomposite is obtained after drying at 60°C.

Other prepared samples GA, GP and GM are incorporated with CuO by performing same synthesis steps.

3.6 Photo-catalytic experiments:

Photo-catalytic activity of as prepared samples is analyzed under UV light exposure by using methylene blue (MB) as a target. Aqueous solution of MB is prepared with the concentration of 0.01g/L in a beaker. Temperature of the photo-catalytic reactor is kept in control by an external cooling jacket with recycled water.

3.6.1   Photo-catalytic Activity of Graphene Oxide (GO):

0.05g of as prepared graphene oxide is dispersed in 50ml of aqueous solution of MB. Catalytic reaction is started by exposure of UV light in photo-catalytic reactor. Suspension is continuously stirred to reach the adsorption-desorption equilibration. After every 1h, some amount of suspension is collected and centrifuged to monitor the degradation of MB.

3.6.2   Photo-catalytic Activity of Graphene (GA):

As prepared graphene sample GA (0.05mg) is dispersed in aqueous solution of MB (50ml). Catalytic reaction is started with the irradiation of UV light in photo-catalytic reactor. Suspension is continuously stirred to attain the adsorption-desorption equilibrium. After every 1h, some amount of suspension is removed from the reactor and centrifuged to measure the degradation of MB.

3.6.3   Photo-catalytic Activity of copper oxide (CuO):

Copper oxide (CuO) (0.05mg) is dispersed in aqueous solution of MB (50ml). To start the catalytic reaction, solution is exposed to UV light in photo-catalytic reactor. Suspension is continuously stirred to reach the adsorption-desorption equilibration. After every 1h, some amount of suspension is collected and centrifuged to analyze the degradation of MB.

3.6.4   Photo-catalytic Activity of GO/CuO nanocomposite:

0.05g of as prepared GO/CuO nanocomposite is dissolved in the 50ml of aqueous solution of MB. Catalytic reaction is started by exposure of UV light in photo-catalytic reactor. Suspension is continuously stirred to achieve the adsorption-desorption equilibrium. After every 1h, some amount of suspension is withdrawn and centrifuged to remove solid material from the solution for further analysis of MB degradation.

3.6.5   Photo-catalytic Activity of GA/CuO nanocomposite:

As synthesized GA/CuO (0.05mg) nanocomposite is dispersed in aqueous solution of MB (50ml). Catalytic reaction is started by irradiation of UV light in photo-catalytic reactor. Continuous stirring is given to the suspension to reach the adsorption-desorption equilibration. After every 1h, some amount of suspension is collected and centrifuged to remove solid material from the solution to further analyze the degradation of MB.

Chapter No.4

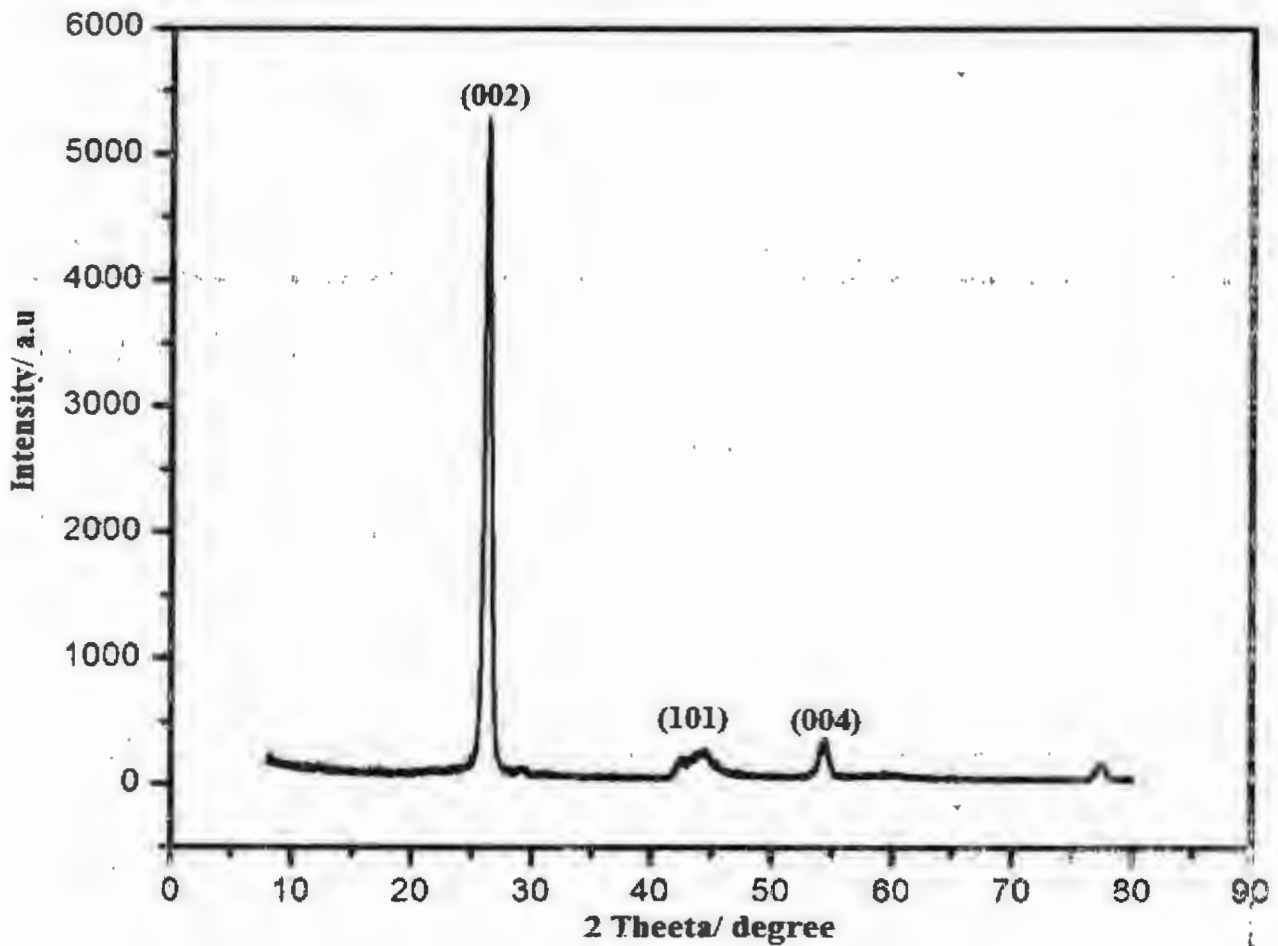# Results and Discussion

4.1 X- Ray Diffraction Spectroscopy:
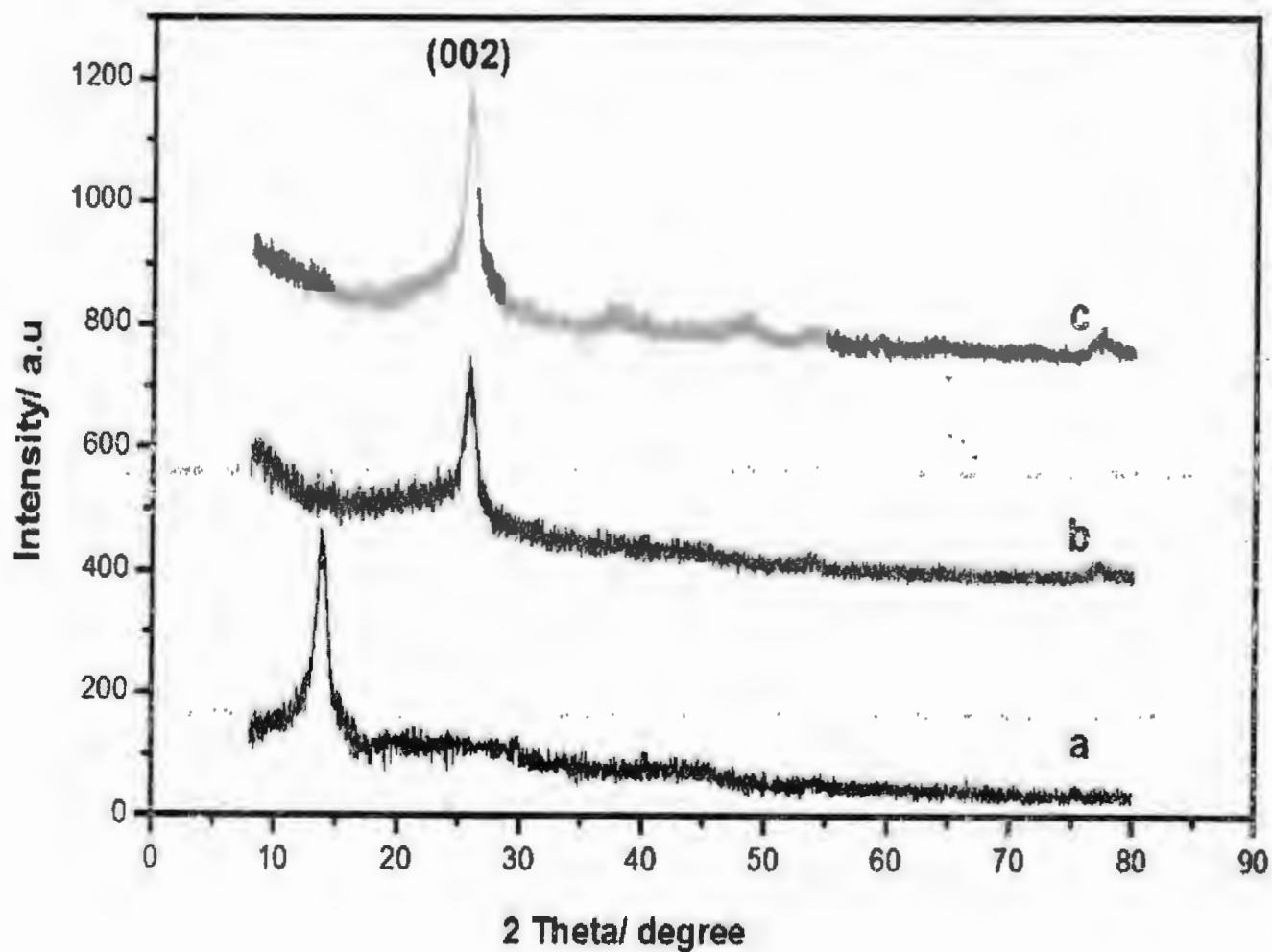

Figure 4.1: XRD spectrum of natural graphite.

34

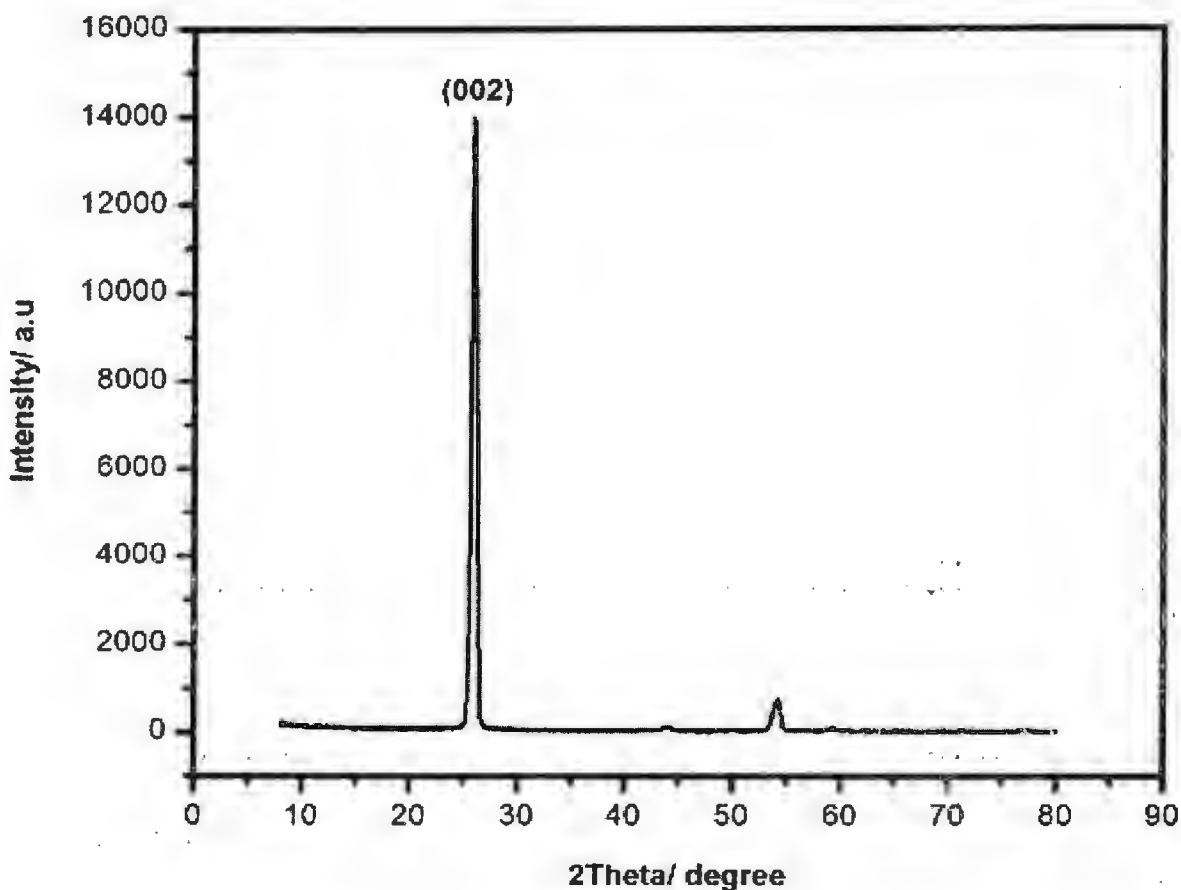**Figure 4.2:** XRD pattern of **(a)** GO, **(b)** GP and **(c)** GA

Figure 4.3: XRD pattern of GM.

X-Ray Diffraction characterization technique used for the structural analysis of the samples. Figure 4.1 is the XRD pattern of natural graphite, graphite has sharp and strong diffraction peak at $2\theta = 26.25°$ having d-spacing distance of 0.34nm corresponds to the (002) reflection of graphite. This intense peak represents the highly ordered crystal structure of graphite. Figure 4.2 shows the XRD pattern of (a) GO, (b) GP and (c) GA. (a) revealed that after chemical oxidation and exfoliation (002) peak shifted towards the lower angle $2\theta = 10.89°$ with an increase in d-spacing value from 0.34nm to 0.88nm. This

increase in d-spacing distance is attributed to the intercalation of oxygen functional groups in to the graphite layered structure. This intercalated oxygen expands the graphene oxide lattice and thus weaken the interlayer van der Waals interaction between the layers compared with that of graphite. Fu, C, *et al*, [88] XRD results confirmed that, after oxidation diffraction peak (002) of graphite at $2\theta = 26.58°$ shifted to the smaller angle $2\theta = 11.42°$ with an increased d-spacing value of 0.774nm. After reduction treatment of graphene oxide figure 4.2 (b, c), graphene nanosheets exhibits the diffraction peak at $2\theta = 25.81°$ along (002) orientation, corresponding to the d-spacing distance of 0.35nm. This d-spacing value is slightly greater than that of well-ordered natural graphite, which might be due to the presence of small amount of residual oxygen-containing functional groups or other structural defects. Yan J, *et al*, [89] synthesized graphene nanosheets exhibits a diffraction peak (002) at $2\theta = 24.8°$ representing an interlayer spacing of 0.36 nm. By comparing the intensities of graphene samples figure 4.2 (b) and figure 4.2 (c), intensity of GA is greater with (002) plane at $2\theta = 25.81°$ than GP at same angle and with the same plane indicating that graphene prepared by plant extract is more amorphous than graphene prepared by ammonia. Figure 4.3 presents the XRD pattern of GM. Results revealed that, a strong and intense peak appeared at $2\theta = 26.02°$ along (002) orientation with the d-spacing value of 0.34nm. These results approximately match with the XRD pattern of graphite (figure 4.1). As graphite is the starting material and final material also give the results just like graphite hence this method is not successful for the synthesis of graphene nanosheets.

4.2 Scanning Electron Microscopy:

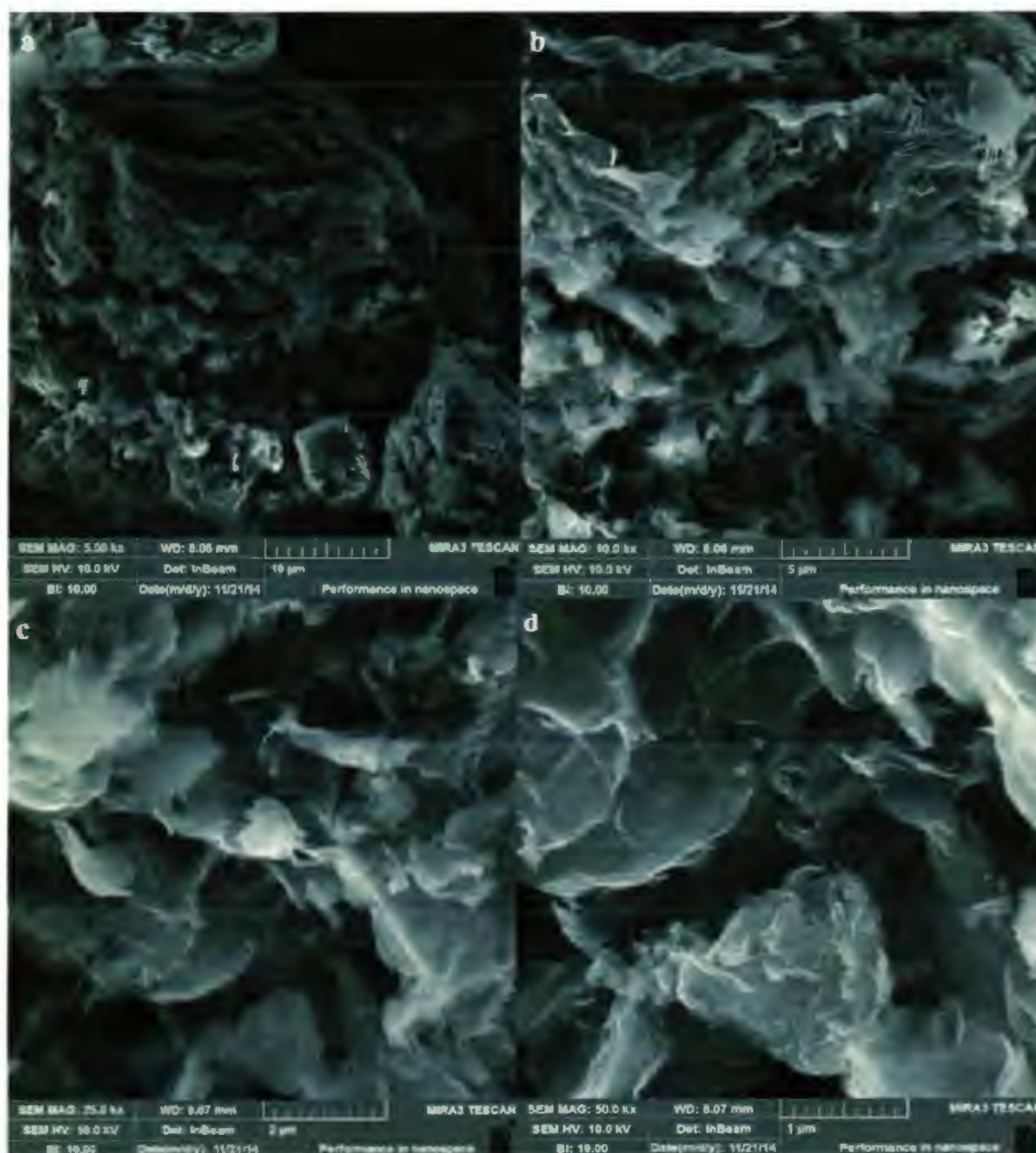Microstructure and morphology of as-synthesized samples were investigated by scanning electron microscopy.

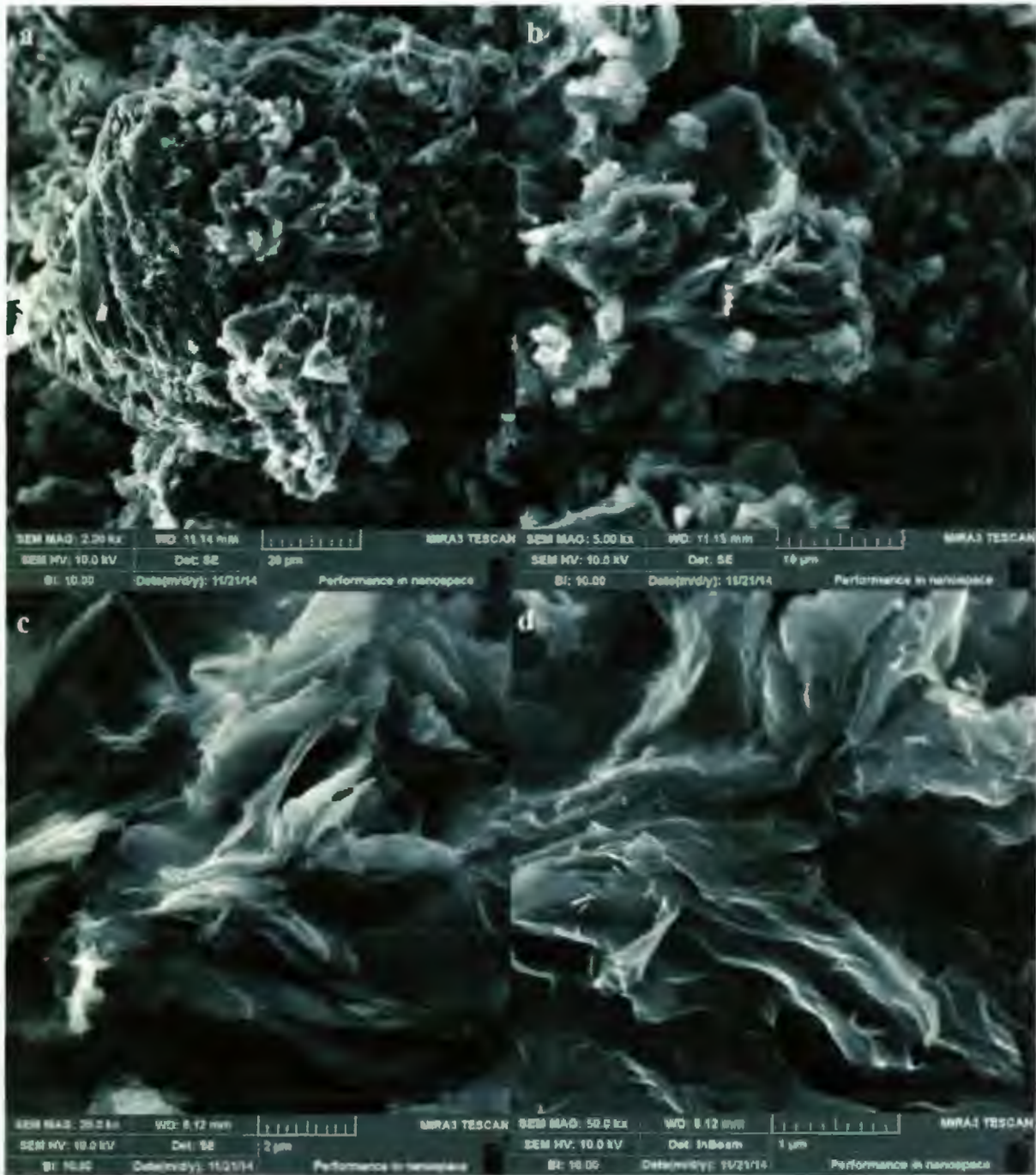**Figure 4.4 (a):** SEM images of GO at different resolutions.

Figure 4.4 (b): SEM images of GA different resolutions.
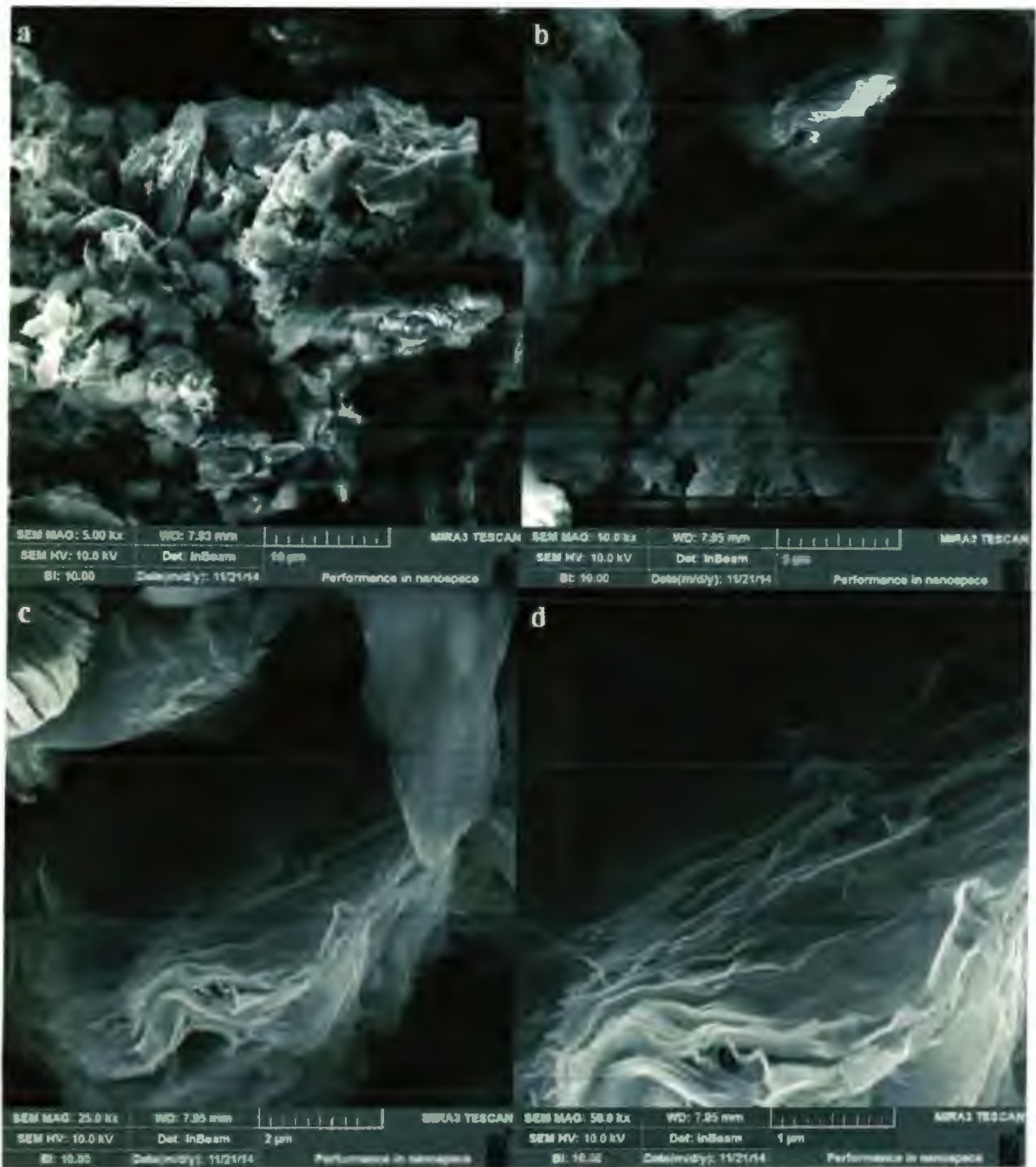
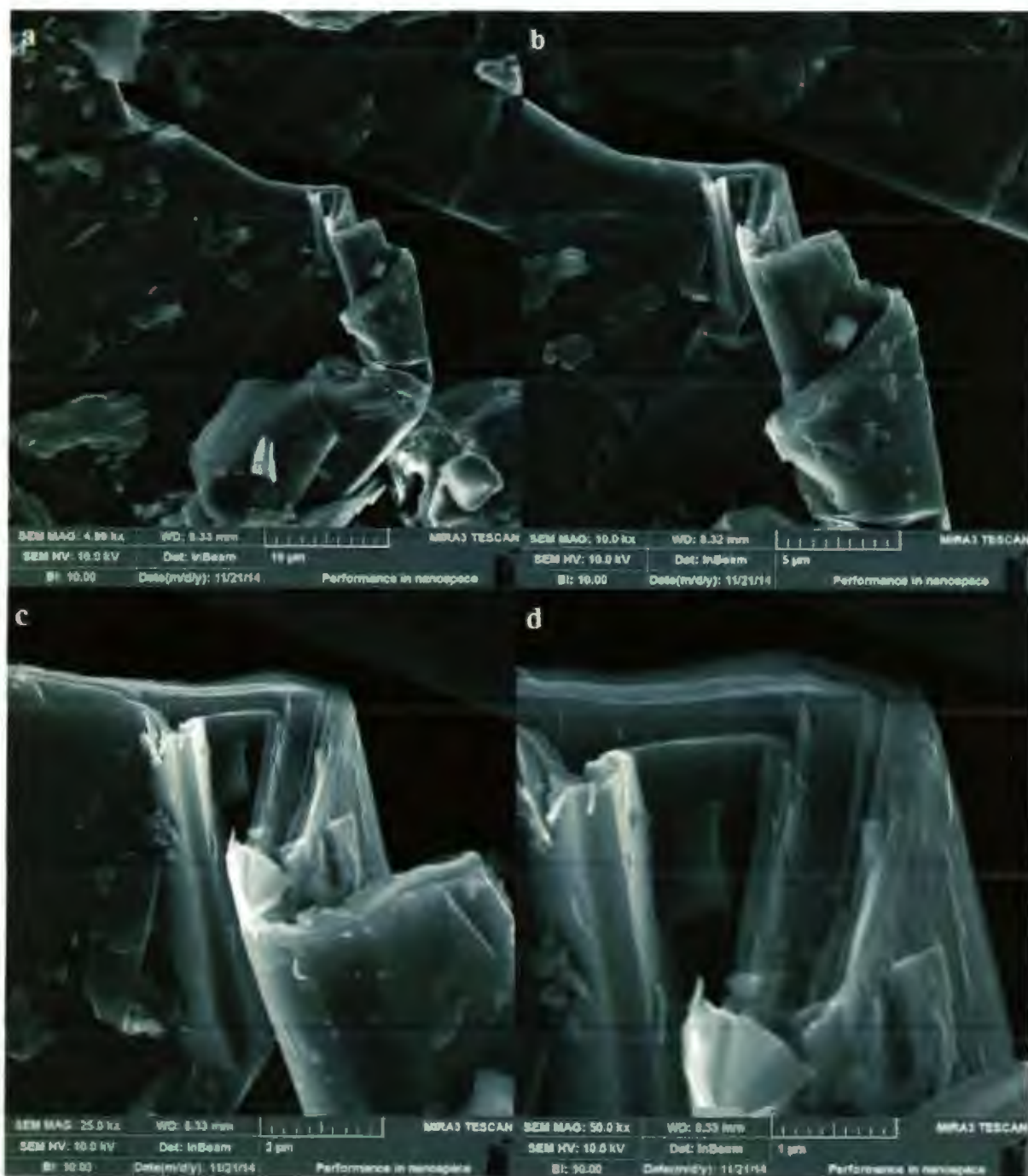**Figure 4.4 (c):** SEM images of GP at different resolutions.

Figure 4.4 (d): SEM images of GM at different resolutions.

Figure 4.4 (a,b,c,d) shows the SEM micrograph of graphene oxide and graphene nanosheets prepared by different methods. Figure 4.4 (a) shows the morphology of GO which revealed that after oxidation and ultrasonication graphene oxide sheets become transparent. Sheets have agglomerated fluffy appearance and decomposition of the oxygen functional groups leads to a disordered stacking of sheets. Figure 4.4 (b,c,d) SEM micrograph of GA, GP and GM respectively. High resolution images of both figure 4.4 (b) and (c) revealed that graphene nanosheets have ultra thin layered, crumpled and wrinkled morphology which is the reason of sheet folding. Wrinkled geometry is the result of $\pi-\pi$ interaction within sheets of graphene which minimizes the surface energy and induces mechanical integrity. Graphene sheets are more transparent than graphene oxide sheets which suggests the successful reduction of graphene oxide in to graphene nanosheets. Figure 4.4 (d) is SEM micrograph of GM. It shows that particles are in the platelet-like crystaline type of structure, which is the morphology of graphite material. As expended graphite is the starting material in this method hence this method did not give the successful synthesis of graphene sheets and it is also explained in XRD results. So graphene sheets can be affectively synthesized from graphite oxide through exfoliation and reduction. Naebe, M, *et al*, [90] prepared graphene sheets from thermal reduction of graphene oxide and functionalization, the results were transparent and wrinkled nanosheets in both cases. Hence functionalization process did not cause the restacking and agglomeration of graphene sheets. Loryuenyong, V, *et al*, [91] prepare the graphene through exfoliation and reduction. SEM results present that, graphite is in the crystalline form of carbon, after oxidation and exfoliation sheets become smaller and transparent. Then after reduction, graphene sheets exhibit wrinkled structure.

4.3 Energy Dispersive Spectroscopy:

Figure 4.5 (a): Energy dispersive spectroscopy spectrum of GO.

Table 4.1 (a) Chemical compositional analysis of GO.

Element	Weight%	Atomic%
C K	74.47	79.53
O K	25.53	20.47
Total	100.00	100.00

Figure 4.5 (b): Energy dispersive spectroscopy spectrum of GA.

Table 4.1 (b) Chemical compositional analysis of GA.

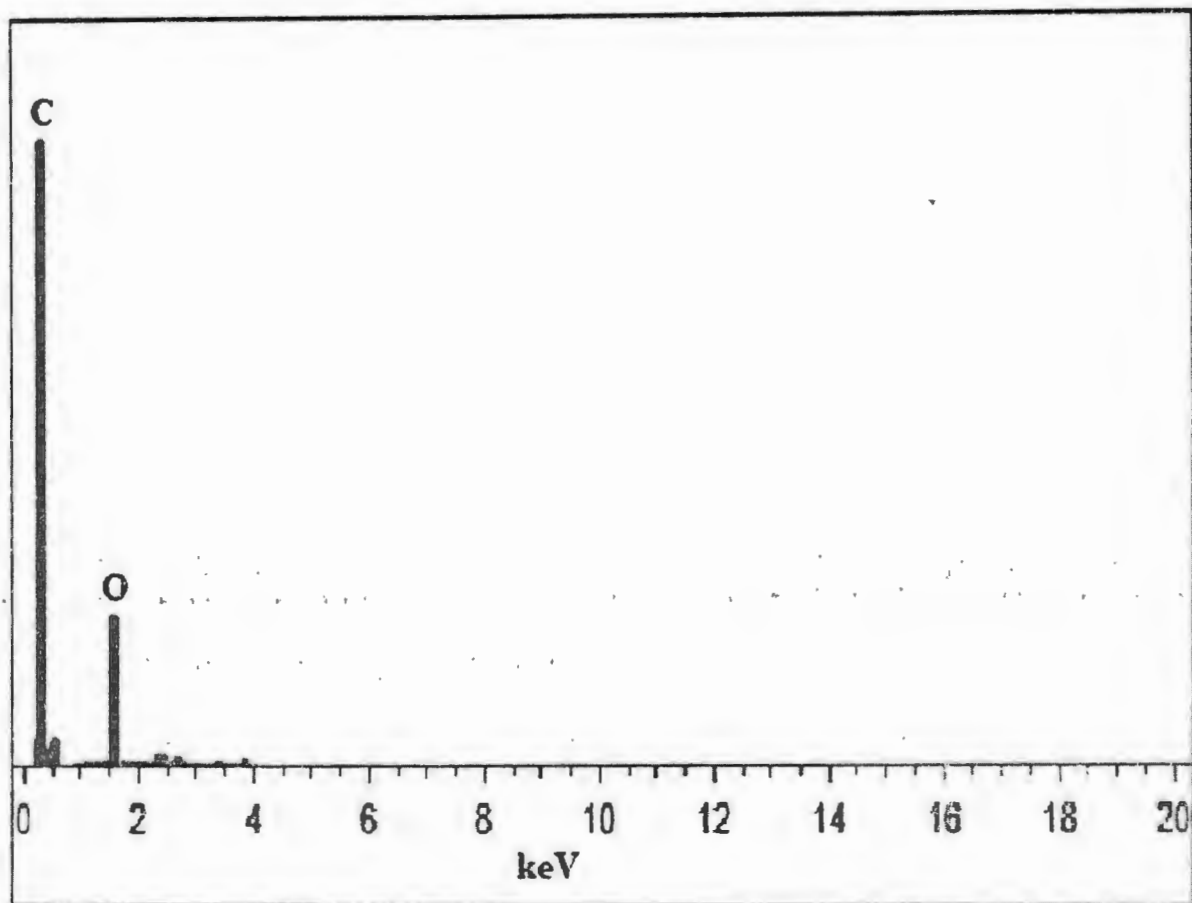| Element	Weight%	Atomic%
C K	90.64	94.89
O K	9.36	5.11
Total	100.00	100.00

Figure 4.5 (c): Energy dispersive spectroscopy spectrum of GP.

Table 4.1 (c) Chemical compositional analysis of GP.

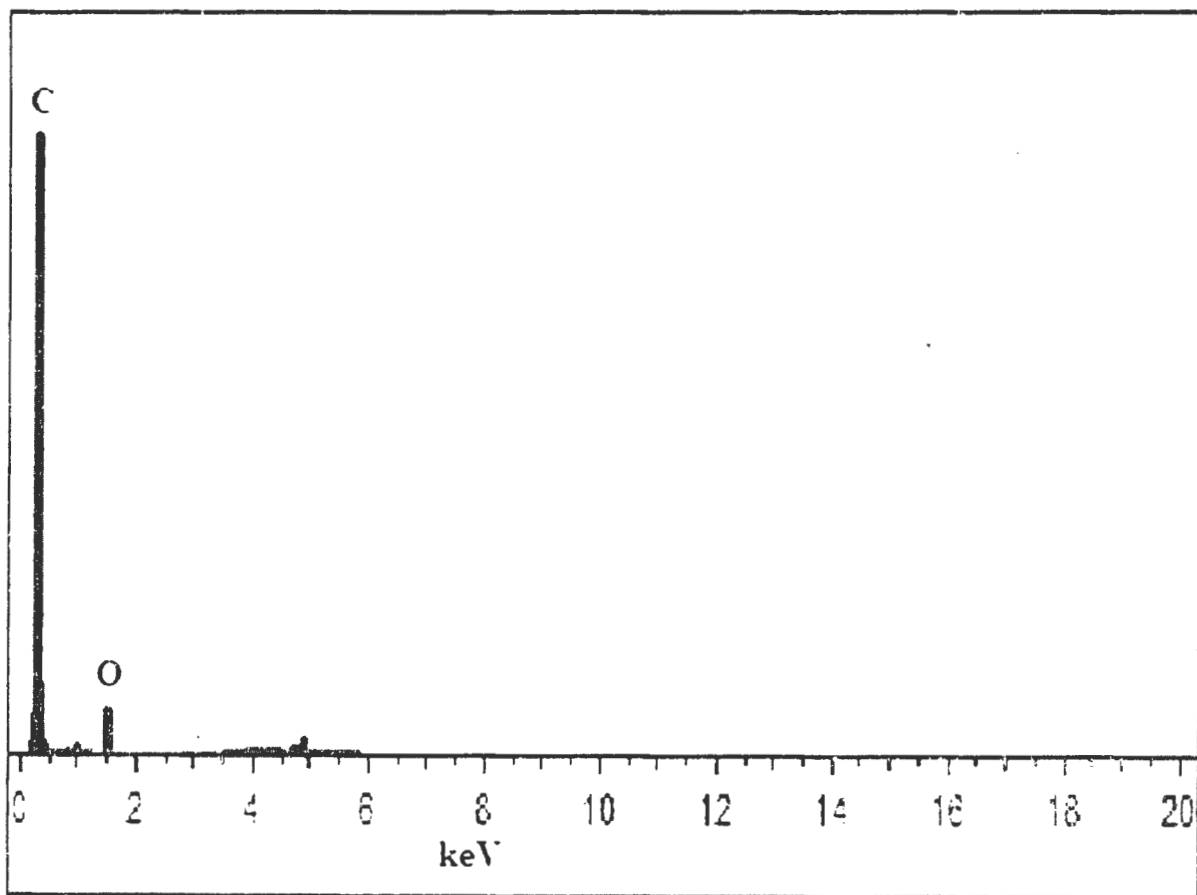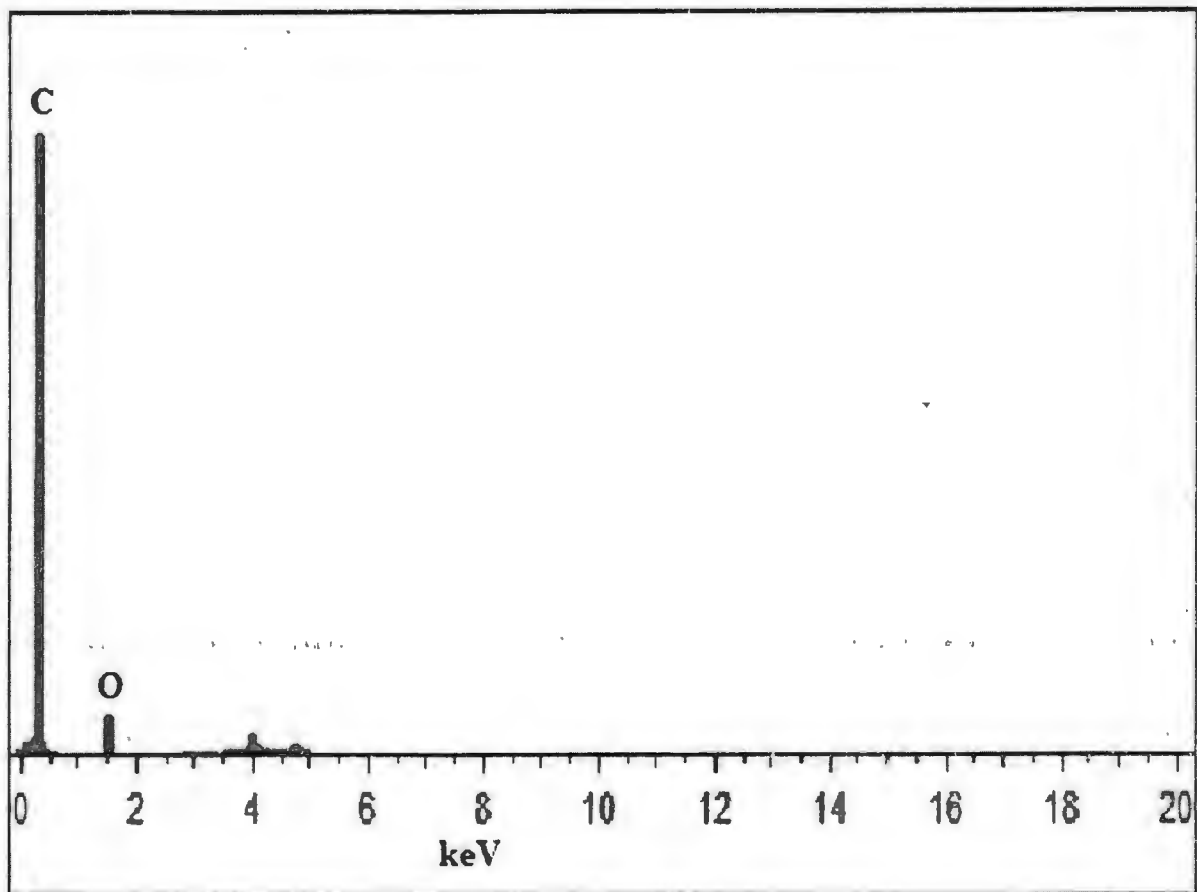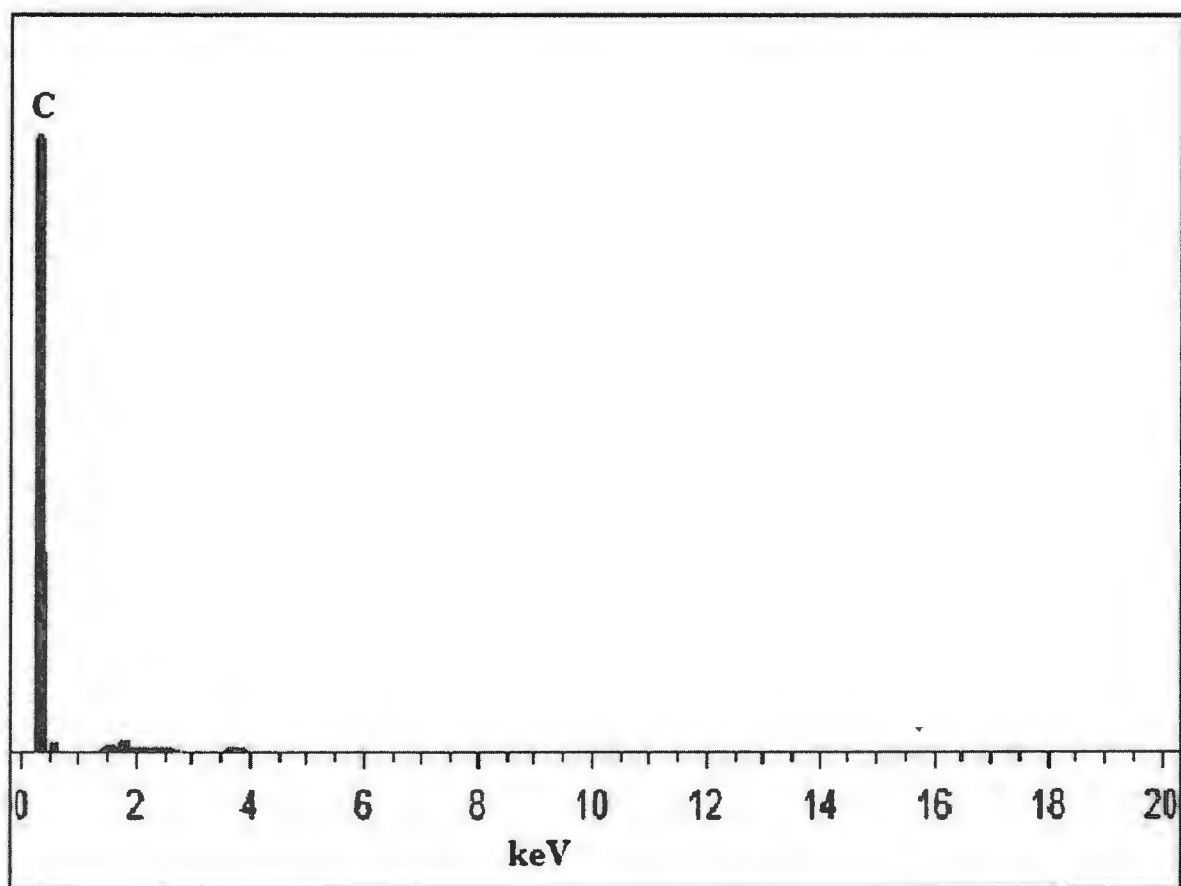| Element	Weight%	Atomic%
C K	91.27	94.71
O K	8.73	5.29
Total	100.00	100.00

45

Figure 4.5 (d): Energy dispersive spectroscopy spectrum of GM.

Table 4.1 (d) Chemical compositional analysis of GM.

Element	Weight%	Atomic%
C K	100.00	100.00
Total	100.00	100.00

Backscattered electrons in SEM display gives the compositional contrast that results from different atomic number elements and their distribution. Energy Dispersive spectroscopy is used to find what those particular elements are and their relative proportions such as weight% and atomic%. In figure 4.5 presents the EDS results of (a) GO, (b) GA, (c) GP and (d) GM. In figure 4.5 (a) EDX analysis confirms the presence of both carbon and oxygen. The EDS spectrum in figure 4.5 (b, c,) confirms the presence of carbon and very small composition of oxygen which is a negligible amount. This compositional analysis explains the reduction of graphene oxide in to graphene nanosheets. In figure 4.5 (d) the EDS spectrum confirms that this prepared sample contains only carbon composition. As explained in XRD and SEM, this method did not give successful synthesis of graphene sheets and starting material graphite has only carbon's composition.
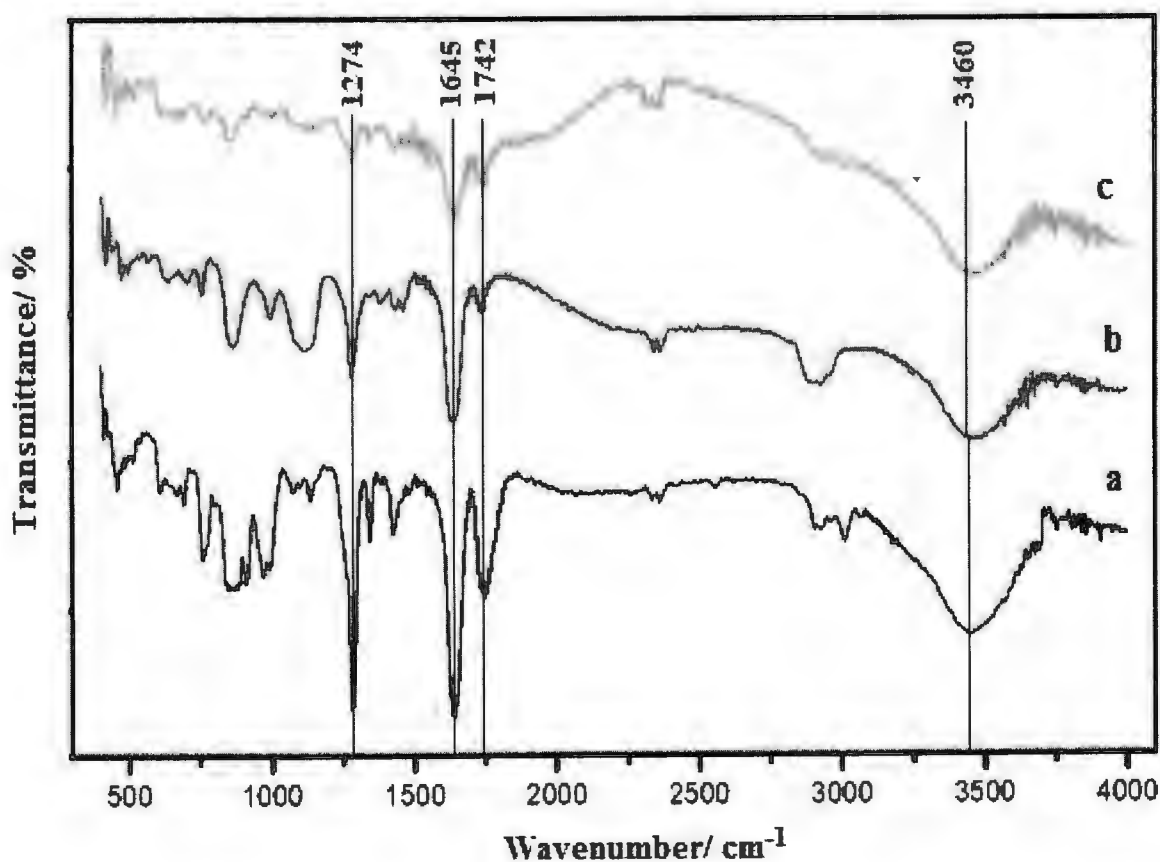
4.4 Fourier Transform Infrared Spectroscopy:

Figure 4.6. FTIR spectra of **(a)** GO, **(b)** GP, **(c)** GA

Figure 4.6 shows the Fourier-Transform Infrared spectroscopy of as prepared samples (a) GO, (b) GP, (c) GA. In Figure 4.6 (a) results of GO indicated that, a broad peak at 3460 cm^{-1} attributed to O–H stretching vibrations of absorbed water molecules and structural OH groups. The peak at 1742 cm^{-1} presents the C=O carbonyl (or carboxyl) stretching. The C–O epoxide group stretching is presented by a peak at 1274 cm^{-1}. The spectra show another peak at 1645 cm^{-1} which is attributed to C=C stretching vibrations from unoxidized graphitic domains. The high intensity of the main peaks in GO shows the presence of a large amount of oxygen functional groups, which confirms the oxidation of graphite. Shahriary, L, *et al,* [92] observed a broad peak between 3000 –3700 cm^{-1} attributed to the stretching vibration of O–H groups of adsorbed water molecules on graphene oxide. Peak appear at 1630 cm^{-1} presents the stretching vibration of C=C. The absorption peak at 1385 cm^{-1} corresponds to the stretching vibration of C=O of carboxylic acid. These oxygen-containing groups confirms that the graphite has been oxidized. After the GO is reduced, figure 4.6 (b, c) represents that the peaks of these functional groups such as O–H, C=O and C–O become significantly weaker than that of GO. Which indicated that most of the bonds related to oxide groups, such as, O–H, C=O and C–O, decreased dramatically. Thus FTIR spectroscopy confirms the reduction process of graphene oxide. But C=C stretching is still present after reduction at 1645cm^{-1}. Justin, R, *et al,* [93] investigated that peak intensities of C–O bonds at 1050–1060 cm^{-1}, the C=O bonds at 1700–1750 cm^{-1} and the O–H bonds at 3400 cm^{-1} become smaller after reduction.

4.5 Photo-catalytic Activity:

Photo-catalytic activities of as-prepared graphene, Graphene oxide, Graphene/CuO, GO/CuO and pure CuO are studied by the decomposition of MB used as a model target organic pollutant under UV light irradiation.

When synthesized graphene sample used as a catalyst, it is observed that after 120 min of reaction time 99.9% of dyes are degraded. This result can be seen in the following photographic image.

Figure 4.7: Methylene blue solution under the photo-catalytic effect of graphene with UV light after **(a)** 0, **(b)** 60 and **(c)** 120 min

When MB is degraded under the effect of graphene oxide, 90% of initial concentration is decomposed from the solution after 120 min. This result can be observed in the following photographic image.

Figure 4.8: Methylene blue solution under the photo-catalytic effect of graphene oxide with UV light after **(a)** 0, **(b)** 60 and **(c)** 120 min

When as-prepared graphene/CuO nanocomposite used as a catalyst, it is revealed that after 120 min of reaction time 96.8% of dyes are degraded. This result is shown in the following photographic image.
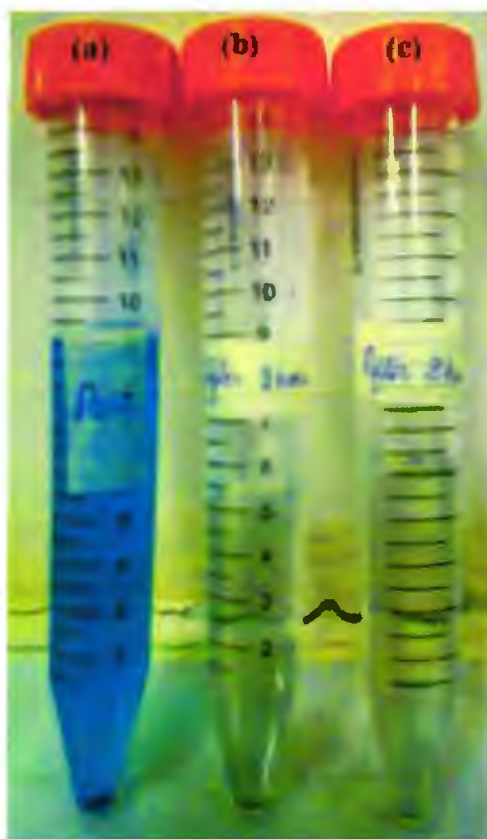

Figure 4.9: Methylene blue solution under the photo-catalytic effect of Graphene/CuO with UV light after **(a)** 0, **(b)** 60 and **(c)** 120 min

When methylene blue solution under the photo-catalytic effect of GO/CuO nanocomposite is evaluated, it is revealed that 76.9% of initial concentration is degraded after 120 min. This result can be observed in the following photographic image.
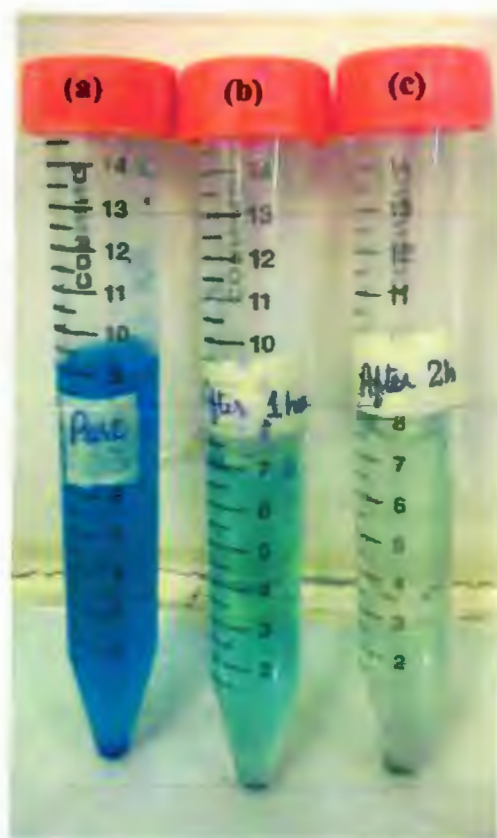

Figure 4.10: Methylene blue solution under the photo-catalytic effect of GO/CuO with UV light after **(a)** 0, **(b)** 60 and **(c)** 120 min

When methylene blue solution is observed under the photo-catalytic effect of pure CuO with the UV light irradiation, it is revealed that 49.9% of dyes is decomposed from the solution after 120 min of illumination. This result can be seen in the following photographic image.
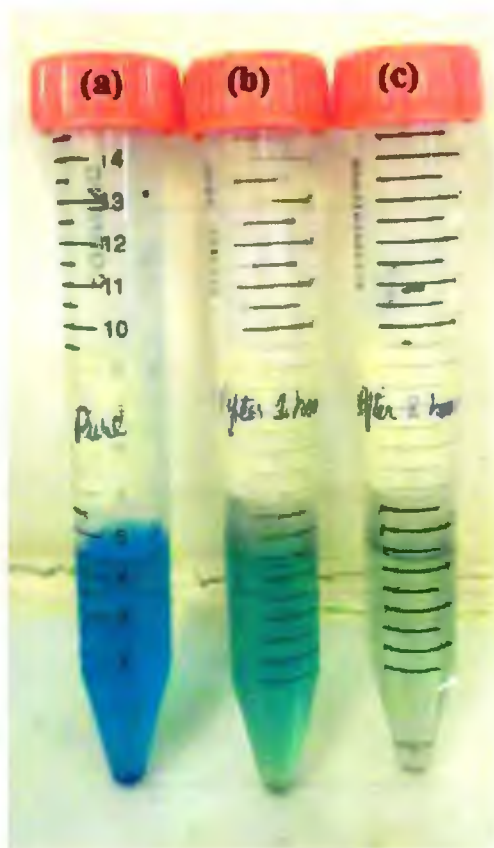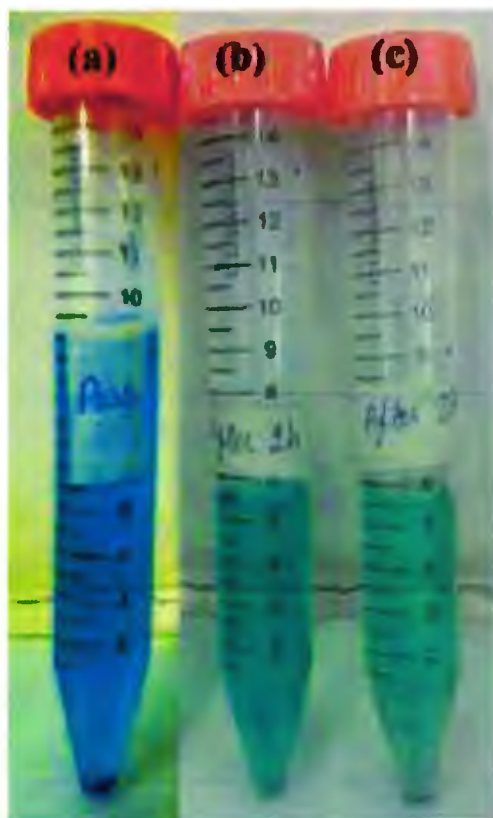

Figure 4.11: Methylene blue solution under the photo-catalytic effect of CuO with UV light after **(a)** 0, **(b)** 60 and **(c)** 120 min
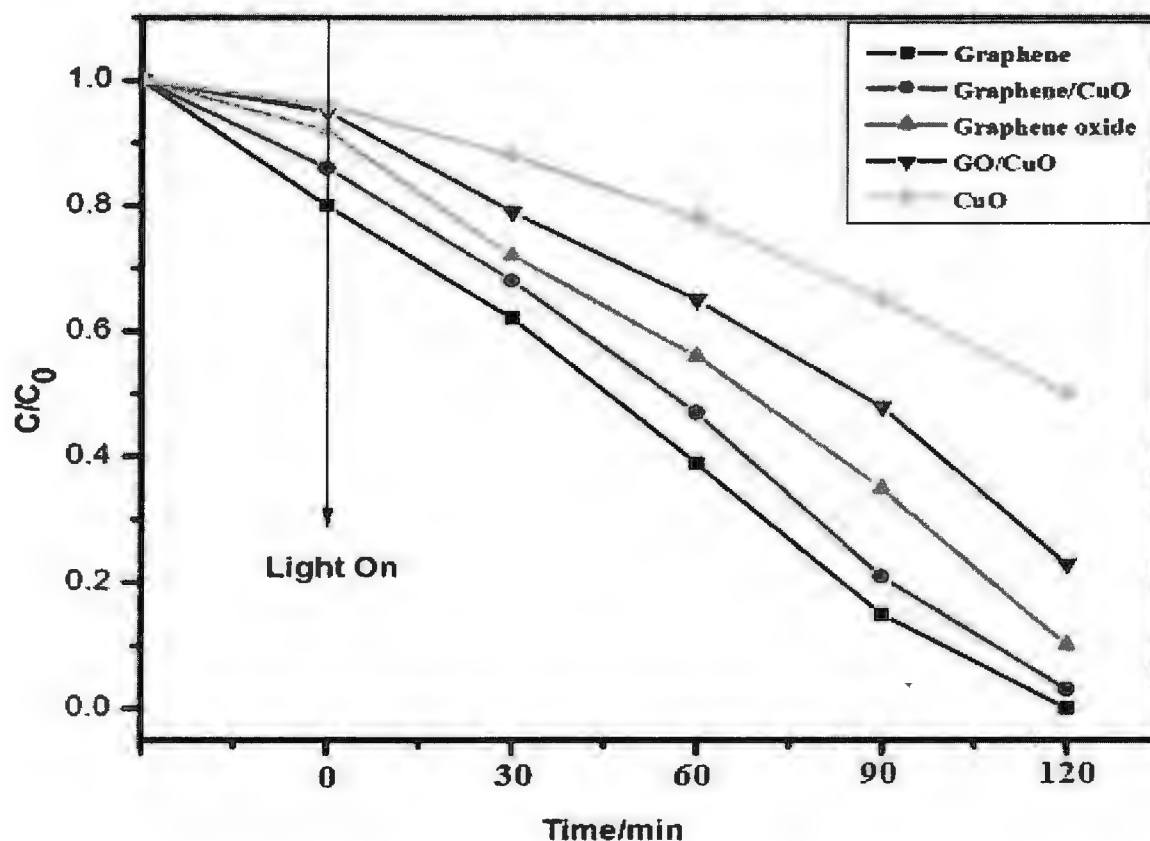
Figure 4.12: Relative concentration (C/C_0) of MB versus time under UV-light irradiation with Graphene, Graphene/CuO, GO, GO/CuO and CuO as photo-catalysts.

In figure 4.8 Photo-catalytic activity of Graphene, GO, Graphene/CuO, GO/CuO and pure CuO are investigated in comparison by the degradation of MB under UV light at room temperature. Results indicated that 99.9% of dyes are removed from the solution after 120 min of irradiation in the presence of graphene catalyst. When graphene oxide is used as a catalyst it degrade 90% of initial MB concentration. In comparison, pure CuO nanoparticle decomposed only 49.9% of MB under same testing conditions. GO/CuO and graphene/CuO nanocomposite exhibits a remarkable photo-catalytic degradation efficiency of MB compared with the pure CuO nanoparticles. Under UV light illumination for 120 min, 76.9% of the initial MB dyes are decomposed by using the GO/CuO nanocomposites and 96.8% of initial

MB are degraded by graphene/CuO nanocomposite, Above observation indicated that the introduction of graphene plays an active part in the catalytic degradation process of dyes.

Two most important factors which determine the efficiency of the photo-catalytic reaction are, efficient adsorption of dye molecules on the photo-catalysts and effective separation of photo-generated electron/hole pairs. When light is irradiated, valence electrons of CuO are excited to the conduction band. These photo-generated electrons are transferred to the graphene and act as electron trap. Trapped electrons on graphene can react with the dissolved oxygen to form reactive oxygen species. Hence rate of electron-hole recombination decreases. [82]. Photo-generated electrons on CuO surface can also be trapped directly by the dissolved oxygen to form reactive oxygen species and these reactive oxygen species react with water to create hydroxyl radicals. MB is then degraded by these hydroxyl groups. Moreover, holes on the valence band of CuO react with absorbed water or hydroxyl groups to form surface hydroxyl radicals which can also decompose the dye. Besides this, holes can also oxidize the dye molecules directly [63].

Conclusions

- Graphene nanosheets are successfully synthesized by Hummers method in comparison with microwave synthesis method.

- X-ray diffraction results confirmed that graphene oxide is successfully reduced to graphene nanosheets, because oxidation peak shifted from $2\theta = 11.42°$ to the higher angle $2\theta = 25.77°$ with decrease in de-spacing value.

- Scanning electron microscopy revealed that graphene oxide sheets are less transparent and stacked together. After reduction graphene nanosheets become more transparent and exhibits wrinkled morphology.

- Fourier transform infrared spectroscopy confirmed the successful oxidation of graphite in to graphene oxide and also reduction process of graphene oxide because bonds related to oxide groups decreases after reduction.

- Graphene oxide/ copper oxide and graphene/ copper oxide nanocomposites are successfully synthesized for photo-catalytic applications. Nanocomposites exhibit more photo-catalytic response than pure CuO.

- Present project could pave the way towards the enhanced photo-catalytic activity of metal oxides by incorporating them with graphene nanosheets. These nanocomposites have potential applications in water treatment, sensors, and energy storage.

References

[1]   R. P. Feynman, Microelectromechanical Systems, Journal of 1 (1992) 60.

[2]   G. M. Whitesides, Small 1 (2005) 172.

[3]   M. I. Katsnelson, Materials Today 10 (2007) 20.

[4]   A. Hirsch, Nat Mater 9 (2010) 868.

[5]   S. Mallakpour, A. Abdolmaleki, and S. Borandeh, Applied Surface Science 307 (2014) 533.

[6]   Z.-S. Wu, G. Zhou, L.-C. Yin, W. Ren, F. Li, and H.-M. Cheng, Nano Energy 1 (2012) 107.

[7]   Nat Mater 9 (2010) 867.

[8]   M. Terrones, A. R. Botello-Méndez, J. Campos-Delgado, F. López-Urías, Y. I. Vega-Cantú, F. J. Rodríguez-Macías, A. L. Elías, E. Muñoz-Sandoval, A. G. Cano-Márquez, J.-C. Charlier, and H. Terrones, Nano Today 5 (2010) 351.

[9]   A. H. Castro Neto, F. Guinea, N. M. R. Peres, K. S. Novoselov, and A. K. Geim, Reviews of Modern Physics 81 (2009) 109.

[10]   W.-W. Liu, S.-P. Chai, A. R. Mohamed, and U. Hashim, Journal of Industrial and Engineering Chemistry 20 (2014) 1171.

[11]   G. Mittal, V. Dhand, K. Y. Rhee, S.-J. Park, and W. R. Lee, Journal of Industrial and Engineering Chemistry

[12]   S. Reich and C. Thomsen, Philosophical Transactions of the Royal Society of London. Series A: Mathematical, Physical and Engineering Sciences 362 (2004) 2271.

[13]   P. R. Wallace, Physical Review 71 (1947) 622.

[14]   F. Barroso-Bujans, S. Cerveny, R. Verdejo, J. J. del Val, J. M. Alberdi, A. Alegría, and J. Colmenero, Carbon 48 (2010) 1079.

[15]   S. M. Singh Chauhan and S. Mishra, Molecules 16 (2011) 7256.

[16]   J. A. Johnson, C. J. Benmore, S. Stankovich, and R. S. Ruoff, Carbon 47 (2009) 2239.

[17]   S. Park and R. S. Ruoff, Nat Nano 4 (2009) 217.

[18]   M. Pumera, Electrochemistry Communications 36 (2013) 14.

[19]   S. Muhammad Hafiz, R. Ritikos, T. J. Whitcher, N. Md. Razib, D. C. S. Bien, N. Chanlek, H. Nakajima, T. Saisopa, P. Songsiriritthigul, N. M. Huang, and S. A. Rahman, Sensors and Actuators B: Chemical 193 (2014) 692.

[20] C. Xu, R.-s. Yuan, and X. Wang, New Carbon Materials 29 (2014) 61.

[21] S. Basu and P. Bhattacharyya, Sensors and Actuators B: Chemical 173 (2012) 1.

[22] H. S. Sim, T. A. Kim, K. H. Lee, and M. Park, Materials Letters 89 (2012) 343.

[23] A. K. Geim and K. S. Novoselov, Nat Mater 6 (2007) 183.

[24] M. Dvorak, W. Oswald, and Z. Wu, Sci. Rep. 3 (2013)

[25] J. Liu, L. Cui, and D. Losic, Acta Biomaterialia 9 (2013) 9243.

[26] M. D. Stoller, S. Park, Y. Zhu, J. An, and R. S. Ruoff, Nano letters 8 (2008) 3498.

[27] C. Lee, X. Wei, J. W. Kysar, and J. Hone, Science 321 (2008) 385.

[28] A. A. Balandin, S. Ghosh, W. Bao, I. Calizo, D. Teweldebrhan, F. Miao, and C. N. Lau, Nano letters 8 (2008) 902.

[29] K. I. Bolotin, K. Sikes, Z. Jiang, M. Klima, G. Fudenberg, J. Hone, P. Kim, and H. Stormer, Solid State Communications 146 (2008) 351.

[30] A. Martín and A. Escarpa, TrAC Trends in Analytical Chemistry 56 (2014) 13.

[31] S. Y. Toh, K. S. Loh, S. K. Kamarudin, and W. R. W. Daud, Chemical Engineering Journal 251 (2014) 422.

[32] C.-T. Hsieh, Y.-Y. Liu, and A. K. Roy, Electrochimica Acta 64 (2012) 205.

[33] H.-H. Chang, C.-K. Chang, Y.-C. Tsai, and C.-S. Liao, Carbon 50 (2012) 2331.

[34] M. A. Raj and S. A. John, Analytica Chimica Acta 771 (2013) 14.

[35] D. Wang, W. Yan, S. H. Vijapur, and G. G. Botte, Electrochimica Acta 89 (2013) 732.

[36] Q. Li and P. Hai, Materials Science in Semiconductor Processing 22 (2014) 16.

[37] Q. Liu, J. Shi, and G. Jiang, TrAC Trends in Analytical Chemistry 37 (2012) 1.

[38] K. Hu, D. D. Kulkarni, I. Choi, and V. V. Tsukruk, Progress in Polymer Science 39 (2014) 1934.

[39] C. Riedl, C. Coletti, and U. Starke, Journal of Physics D: Applied Physics 43 (2010) 374009.

[40] C. G. Rocha, M. H. Rümmeli, I. Ibrahim, H. Sevincli, F. Börrnert, J. Kunstmann, A. Bachmatiuk, M. Pötschke, W. Li, S. A. M. Makharza, S. Roche, B. Büchner, and G. Cuniberti, in Graphene, CRC Press, 2011, p. 1.

[41] A. Jorio, M. S. Dresselhaus, R. Saito, and G. Dresselhaus, John Wiley & Sons (2011) 370.

[42] K. F. Mak, L. Ju, F. Wang, and T. F. Heinz, Solid State Communications 152 (2012) 1341.

[43]   K. S. Novoselov, A. K. Geim, S. V. Morozov, D. Jiang, M. I. Katsnelson, I. V. Grigorieva, S. V. Dubonos, and A. A. Firsov, Nature 438 (2005) 197.

[44]   R. Garg, N. Dutta, and N. Choudhury, Nanomaterials 4 (2014) 267.

[45]   M. Edward and K. Mikito, Report on Progress in Physics 76 (2013)

[46]   F. Ducastelle, Physical Review B 88 (2013) 075413.

[47]   I. W. Frank, D. M. Tanenbaum, A. M. van der Zande, and P. L. McEuen, Journal of Vacuum Science & Technology B 25 (2007) 2558.

[48]   Y. Zhu, S. Murali, W. Cai, X. Li, J. W. Suk, J. R. Potts, and R. S. Ruoff, Advanced Materials 22 (2010) 3906.

[49]   S. Goenka, V. Sant, and S. Sant, Journal of Controlled Release 173 (2014) 75.

[50]   V. Singh, D. Joung, L. Zhai, S. Das, S. I. Khondaker, and S. Seal, Progress in Materials Science 56 (2011) 1178.

[51]   Z. Fan, D. Z. Y. Tng, C. X. T. Lim, P. Liu, S. T. Nguyen, P. Xiao, A. Marconnet, C. Y. H. Lim, and H. M. Duong, Colloids and Surfaces A: Physicochemical and Engineering Aspects 445 (2014) 48.

[52]   E. Pop, V. Varshney, and A. K. Roy, MRS Bulletin 37 (2012) 1273.

[53]   K. M. F. Shahil and A. A. Balandin, Solid State Communications 152 (2012) 1331.

[54]   T.-F. Yeh, J. Cihlář, C.-Y. Chang, C. Cheng, and H. Teng, Materials Today 16 (2013) 78.

[55]   Y. Tang, Z. Yang, and X. Dai, Journal of Magnetism and Magnetic Materials 323 (2011) 2441.

[56]   R. R. Nair, M. Sepioni, I. L. Tsai, O. Lehtinen, J. Keinonen, A. V. Krasheninnikov, T. Thomson, A. K. Geim, and I. V. Grigorieva, Nat Phys 8 (2012) 199.

[57]   J. Luo, Journal of Magnetism and Magnetic Materials 366 (2014) 28.

[58]   H. Kumazaki and D. S. Hirashima, Journal of the Physical Society of Japan 76 (2007) 064713.

[59]   R. P. Wijesundera, M. Hidaka, K. Koga, J.-Y. Choi, and N. E. Sung, Ceramics-Silikaty 54 (2010) 19.

[60]   M. Suleiman, M. Mousa, A. Hussein, B. Hammouti, T. B. Hadda, and I. Warad,

[61]   S. Zaman, A. Zainelabdin, G. Amin, O. Nur, and M. Willander, Journal of Physics and Chemistry of Solids 73 (2012) 1320.

[62] M. Ahmad, E. Ahmed, W. Ahmed, A. Elhissi, Z. L. Hong, and N. R. Khalid, Ceramics International 40 (2014) 10085.

[63] A. Wang, X. Li, Y. Zhao, W. Wu, J. Chen, and H. Meng, Powder Technology 261 (2014) 42.

[64] J. Liu, Z. Liu, C. J. Barrow, and W. Yang, Analytica Chimica Acta

[65] A. S. Ethiraj and D. J. Kang, Nanoscale Research Letters 7 (2012) 70.

[66] X. An, K. Li, and J. Tang, ChemSusChem 7 (2014) 1086.

[67] Z.-g. Wang, P.-j. Li, Y.-f. Chen, J.-r. He, B.-j. Zheng, J.-b. Liu, and F. Qi, Materials Letters 116 (2014) 416.

[68] W. Yuan, B. Li, and L. Li, Applied Surface Science 257 (2011) 10183.

[69] T. Wu, J. Gao, X. Xu, W. Wang, C. Gao, and H. Qiu, Nanotechnology 24 (2013) 0957.

[70] K. Wang, T. Feng, M. Qian, H. Ding, Y. Chen, and Z. Sun, Applied Surface Science 257 (2011) 5808.

[71] C. Orofeo, H. Ago, B. Hu, and M. Tsuji, Nano Research 4 (2011) 531.

[72] X. Li, W. Cai, I. H. Jung, J. H. An, D. Yang, A. Velamakanni, R. Piner, L. Colombo, and R. S. Ruoff, ECS Transactions 19 (2009) 41.

[73] V. Krasnenko, J. Kikas, and M. G. Brik, Physica B: Condensed Matter 407 (2012) 4557.

[74] J. Zhao, S.-S. Yang, L.-Q. Chen, Z.-C. Zhang, and H.-L. Zheng, Thin Solid Films 527 (2013) 120.

[75] Y. Wang, Y. Li, L. Tang, J. Lu, and J. Li, Electrochemistry Communications 11 (2009) 889.

[76] Y.-X. Wang, S.-L. Chou, H.-K. Liu, and S.-X. Dou, Carbon 57 (2013) 202.

[77] K. Anand, O. Singh, M. P. Singh, J. Kaur, and R. C. Singh, Sensors and Actuators B: Chemical 195 (2014) 409.

[78] F. Li, Z. Lin, B. Zhang, Y. Zhang, C. Wu, and T. Guo, Organic Electronics 14 (2013) 2139.

[79] J. Cao, Y. Wang, Y. Zhou, J.-H. Ouyang, D. Jia, and L. Guo, Journal of Electroanalytical Chemistry 689 (2013) 201.

[80] K. Cheng, D. He, T. Peng, H. Lv, M. Pan, and S. Mu, Electrochimica Acta 132 (2014) 356.

[81] Y. Qian, F. Ye, J. Xu, and Z.-G. Le, International Journal of Electrochemical Science 7 (2012)

[82] A. Abulizi, G.-H. Yang, and J.-J. Zhu, Ultrasonics Sonochemistry 21 (2014) 129.

REFRENCES

[83]   Y. J. Yang, W. Li, and X. Wu, Electrochimica Acta 123 (2014) 260.

[84]   X. Rong, F. Qiu, C. Zhang, L. Fu, Y. Wang, and D. Yang, Ceramics International 41 (2015) 2502.

[85]   X. Zhou, X. Wang, B. Wang, Z. Chen, C. He, and Y. Wu, Sensors and Actuators B: Chemical 193 (2014) 340.

[86]   Y.-C. Lin, Y. Cao, J.-H. Jang, C.-M. Shu, C. Webb, and W.-P. Pan, Journal of Thermal Analysis and Calorimetry 116 (2014) 1249.

[87]   I. Janowska, K. Chizari, O. Ersen, S. Zafeiratos, D. Soubane, V. Costa, V. Speisser, C. Boeglin, M. Houllé, D. Bégin, D. Plee, M.-J. Ledoux, and C. Pham-Huu, Nano Research 3 (2010) 126.

[88]   C. Fu, G. Zhao, H. Zhang, and S. Li, Int. J. Electrochem. Sci 8 (2013) 6269.

[89]   J. Yan, T. Wei, W. Qiao, B. Shao, Q. Zhao, L. Zhang, and Z. Fan, Electrochimica Acta 55 (2010) 6973.

[90]   M. Naebe, J. Wang, A. Amini, H. Khayyam, N. Hameed, L. H. Li, Y. Chen, and B. Fox, Sci. Rep. 4 (2014)

[91]   V. Loryuenyong, K. Totepvimarn, P. Eimburanapravat, W. Boonchompoo, and A. Buasri, Advances in Materials Science and Engineering 2013 (2013) 5.

[92]   L. Shahriary and A. A. Athawale, Int. J. Renew. Energy and Env. Engg 2 (2014) 58.

[93]   R. Justin and B. Chen, Mater Sci Eng C Mater Biol Appl 34 (2014) 50.